NACA RM L52H22

NACA

RESEARCH MEMORANDUM

AN INVESTIGATION OF SOME FACTORS AFFECTING THE DRAG OF RELATIVELY LARGE NONLIFTING BODIES OF REVOLUTION IN A SLOTTED TRANSONIC WIND TUNNEL

By Robert E. Pendley and Carroll R. Bryan

Langley Aeronautical Laboratory
Langley Field, Va.

NATIONAL ADVISORY COMMITTEE
FOR AERONAUTICS

WASHINGTON

January 15, 1953
Declassified August 21, 1959

NATIONAL ADVISORY COMMITTEE FOR AERONAUTICS

RESEARCH MEMORANDUM

AN INVESTIGATION OF SOME FACTORS AFFECTING THE DRAG OF RELATIVELY LARGE NONLIFTING BODIES OF REVOLUTION IN A SLOTTED TRANSONIC WIND TUNNEL

By Robert E. Pendley and Carroll R. Bryan

SUMMARY

An investigation was conducted to study some factors affecting the drag of relatively large nonlifting bodies of revolution at transonic speeds in the Langley 8-foot transonic tunnel. Drag and surface pressure measurements were made for two geometrically similar bodies of revolution of 8-inch and 4-inch maximum diameter at zero angle of attack through a Mach number range of approximately 0.6 to 1.1. Tunnel-wall Mach number distributions and schlieren photographs also were obtained. In one of the tests, cruciform delta tail fins were added to the larger body.

Analysis of the tests confirmed a result of a prior investigation which had indicated that no significant tunnel-boundary interference should occur at subsonic Mach numbers. A disagreement between the character of the observed subsonic drag rise and that usually observed for fin-stabilized bodies in free flight was shown to be the result of fin interference. Large effects of boundary-reflected disturbances on the drag were found at some supersonic Mach numbers. At the highest test Mach number, however, the boundary interference was such that the drag coefficient of the larger body was approximately equal to that of the smaller body, which was essentially free of tunnel interference at this Mach number. The forebody was nearly free of tunnel interference at the highest test Mach number for the larger body and at Mach numbers greater than about 1.05 for the smaller body.

INTRODUCTION

As a result of the installation of a slotted test section in the Langley 8-foot transonic tunnel (ref. 1), subsonic choking has been

eliminated, and it has become possible to utilize larger models than was formerly feasible. The use of these larger models was considered particularly advantageous for an extensive air-inlet program which had been planned for the Langley 8-foot transonic tunnel, since, in addition to improving the value of the test Reynolds number, the use of larger models expedites the study of the detailed phenomena of ducted-body performance.

Although the investigation reported in reference 2 had indicated no important subsonic interference for a relatively large body in a slotted test section, reference 3 indicated the possibility of appreciable tunnel interference on the drag at supersonic speeds below the Mach number at which the boundary-reflected bow shock clears the model base. It was therefore decided to investigate the effects of this interference in the Langley 8-foot transonic tunnel on the drag of a body of the size of the largest proposed air-inlet body. The body selected was 66 inches long, 8 inches in diameter, and was similar in shape to some of the inlet bodies. Another body which was a half-scale duplicate of the 8-inch body was also used in the investigation in order to observe the effects of the boundary-reflected disturbances at different positions on the body and in order to obtain interference-free data at the highest test Mach number where the boundary-reflected bow shock would clear the model base. It is the purpose of this paper to present the results of this investigation.

During the course of the tests, it was noted that the subsonic drag rise was significantly different from that usually observed in free-flight investigations (for example, ref. 4). It was uncertain whether this difference was caused by subsonic wind-tunnel interference effects not previously observed or by the presence of the stabilizing fins in the free-flight tests. The cause of the difference was therefore investigated by enlarging the wind-tunnel test program to include a configuration comprised of the larger body with cruciform tail fins. The resulting fin-body combination was similar to that for which free-flight data were available in reference 4.

Drag measurements, surface pressure distributions, wind-tunnel wall-pressure distributions, and schlieren photographs were obtained for a Mach number range extending from about 0.6 to 1.1. The investigation was limited to the case for zero angle of attack.

SYMBOLS

B base area, $\frac{d_B{}^2\pi}{4}$

C_D drag coefficient, $\frac{\text{drag}}{q_oF}$

C_{D_b} base drag coefficient, $-P_B \frac{B}{F}$

C_{D_e} balance indication less base drag coefficient, $\frac{G_a}{q_o F} + \frac{P_B B}{F}$

C_{D_f} calculated skin-friction drag coefficient

C_{D_p} pressure drag coefficient, $\int P d(r/R)^2$

d diameter

D body maximum diameter

F fuselage maximum cross-sectional area

G_a axial force indicated by strain-gage balance

H total pressure

L model length

M Mach number

p local static pressure

P pressure coefficient, $\frac{p - p_o}{q_o}$

P_{cr} critical pressure coefficient corresponding to local speed of sound

q dynamic pressure, $\frac{\rho V^2}{2}$

r radius

R body maximum radius

V velocity

x axial distance

α model angle of attack

ρ air density

Subscripts:

o free stream

B model base

APPARATUS AND TESTS

Tunnel.- The test section of the Langley 8-foot transonic tunnel utilized in this investigation was the $\frac{1}{9}$-open slotted test section whose geometry and aerodynamic properties are described in references 1 and 3. Condensation effects in the test section were avoided by maintaining the stagnation temperature sufficiently high by regulation of the quantity of cooling air exchanged.

Figure 1 is a drawing of the model support system used in this investigation. The models were sting-mounted on a steel tube suspended coaxially in the tunnel.

Models.- The coordinates of the two models investigated were derived from those of the body of revolution used in an NACA transonic research program (ref. 5). The forebody of the larger model was designed to have a maximum diameter of 8 inches and a length of four times the maximum diameter. A 2-inch-long cylindrical section connected the forebody to the afterbody. The over-all afterbody length was fixed at seven times the maximum diameter. The rearmost portion of the afterbody was then cut off at a length of approximately 4 diameters. Dimensional coordinates of the two models are given in table I, and important measured over-all dimensions are shown in figure 2.

The external shape of the 4-inch model was designed as a $\frac{1}{2}$-scale model of the 8-inch body. Figure 3 shows the extent to which the 4-inch model simulated the 8-inch model in the region of the model base. A special sting was not manufactured for the 4-inch body. A sting and balance which were used in another investigation were utilized since the proportions of this sting were considered sufficiently close to one-half scale.

Figure 4(a) shows the 8-inch model with tail fins as mounted in the tunnel test section; figure 4(b) shows the 4-inch model and sting and the forebody of the 8-inch model.

The forebody of the 8-inch model was constructed of laminations of Fiberglas cloth covered and impregnated with Paraplex plastic. This

method of construction resulted in a very smooth surface. The afterbody was constructed of $\frac{1}{16}$- inch spun aluminum with all joints and screw holes filled and smoothed to a fair condition. The cylindrical midsection was constructed from $\frac{1}{4}$- inch steel stock. The entire 4-inch body, like the 8-inch forebody, was constructed of laminations of Fiberglas cloth and Paraplex plastic.

Inaccuracies of construction resulted in deviations of the model contours from the design contour. After the tests, the ordinates of the 8-inch forebody and the entire 4-inch model were measured and compared with the ordinates of a curve faired through the design ordinates. The results of this comparison are shown in figure 5 as $\Delta r/L$ (the deviation of the model surface from the faired curve, expressed as a fraction of body length) plotted against longitudinal location. The ordinates of the 8-inch afterbody were not measured as above; local measurements indicated that the surface irregularities were of the order of those measured for the 8-inch forebody.

An alternate 8-inch model was utilized for measurements of circumferential pressure distributions and for runs with transition strips. This model was comprised of the same forebody already described, no midsection, and an afterbody of the design and method of construction identical to that of the one previously described.

Cruciform tail fins were installed on the 8-inch body for one test. The linear dimensions of the fins used in this investigation were approximately equal to those obtained by reducing the dimension of the fins of reference 4 by the ratio of the body maximum diameters. Over-all measured dimensions of the fins are given in figure 2.

Test runs were made with transition strips located on the 4- and the 8-inch models as shown in figure 2. These transition strips consisted of No. 60 carborundum grains secured to the model surface by shellac. The effects of the transition strip on the 8-inch body were obtained by tests of the alternate model fitted with a faired wooden tail cone (fig. 2) with and without the transition strip.

The force balances were of the internal strain-gage type. The design axial load of the balance for the 8-inch model was 170 pounds; for the 4-inch model, this value was 80 pounds. For the pressure tests of the 4-inch model, the balance was removed and a steel tube substituted in order to duct pressure leads into the sting.

Surface pressures on the 8-inch model were measured by means of a row of 0.03-inch-diameter orifices mounted flush with the top surface of the model. The orifices were located longitudinally as shown in table II. A similar row of orifices on the 4-inch model was also located on the top surface of the model. These orifices were 0.022 inch in diameter and were located as shown in table II. Four additional orifice rows spaced at 45° intervals were used on the forebody of the alternate model.

Measuring apparatus.- Pressure measurements were indicated by two 9-foot multiple manometer boards, photographically recorded.

Force readings from the internal strain-gage balance were indicated by a Brown potentiometer and the values manually recorded.

Angle of attack was measured by the use of a cathetometer directed at a line on the side of the model.

Tests.- The investigations were conducted at zero angle of attack through a Mach number range extending from $M = 0.596$ to $M = 1.125$. The Reynolds number range of the tests extended from about 1.1×10^6 to 2.7×10^6 and is indicated in figure 6.

PRECISION

Mach number.- Inaccuracies in the pressure measurements caused a maximum random error in calculating Mach number of no greater than ±0.003. In calculating the local Mach number just outside the boundary layer, the local value of total pressure was assumed equal to the free-stream value. The error thus introduced by neglecting shock losses is negligible at the lower supersonic Mach numbers and did not exceed 0.002 at the highest test Mach number.

As shown in reference 3, the maximum amplitude in the irregularities of the tunnel-center-line Mach number distribution (model absent) was approximately ±0.010 at the higher supersonic Mach numbers. Because of the length of the 8-inch model, it was necessary to place the model in the tunnel so that the nose projected into a region over which the tunnel-empty Mach number distribution (ref. 3) indicated appreciable gradient at the highest test Mach numbers. From the location of the nose to the location of the maximum body diameter, the Mach number increment associated with this gradient amounted to 0.032 at $M_o = 1.13$ and diminished to a negligible amount at $M_o \approx 1.05$. The gradient, however, was distributed such that the larger portion occurred over the forward fifth of model.

Force drag coefficient.- The repeatability of the force measurements indicated that the maximum error in the drag coefficient was probably less than ±0.01.

Pressure coefficient.- The maximum error in pressure coefficient caused by inaccuracies in pressure measurement is estimated as ±0.011.

Pressure drag coefficient.- The errors in the pressure drag coefficients are difficult to assess. The scatter of the data indicates a maximum random error in some instances of about ±0.025, and estimation of the skin-friction coefficient indicated that, for one test, the absolute value of the pressure drag coefficient may also be no more accurate than ±0.025. The changes in the pressure drag coefficients caused by Mach number are believed to be indicated more reliably than the absolute values.

Angle of attack.- The angle of attack was held within ±0.1° of zero.

RESULTS AND DISCUSSION

Tunnel-wall Mach number distributions.- Mach number distributions on a panel of the tunnel wall and on the model surface are shown in figures 7 and 8 for the 8- and 4-inch-diameter bodies, respectively. Tunnel-wall-data points for the 8-inch finned model are shown only when they are appreciably different from the body-alone points. In most cases, the tunnel-empty wall distributions were available for free-stream Mach numbers slightly different from those for which the model-present data are shown. These differences must therefore be kept in mind when examining the data for the effects of the model presence. At high subsonic Mach numbers, the high-pressure region at the nose of the model and the reduced pressures acting over the body surface in the maximum-diameter region were transmitted to the tunnel wall. These pressure perturbations increased with Mach number and were substantially larger for the larger model; the deviations due to the high-pressure region ahead of the model nose were of significant magnitude only for the larger model (figs. 7(b) to 7(d), 8(c), and 8(d)).

At the supersonic Mach numbers, figures 7 and 8 clearly show the extension of model-induced shocks to the tunnel wall. Reflection of the bow shocks from the tunnel wall back to the model is prominently shown at the two highest Mach numbers for both models. The shock configurations sketched on the figures are roughly estimated from reference to schlieren photographs (fig. 9), the tunnel-wall and model-surface Mach number distributions, and the material concerning the location of detached shocks which was discussed in reference 3. Those portions of the shocks

indicated on figures 7 and 8 by solid lines were drawn from reference to the schlieren photographs. The dotted portions of the indicated shock waves are not to be considered as accurate representations of the actual shock configurations.

Mach number effects on surface pressures.- Figures 10 and 11 show a growth in the absolute values of the pressure coefficients over the forebodies of the 8-inch and 4-inch models as the Mach number was increased from about 0.6 to 0.95, at which point local sonic Mach numbers were just attained. An exception to this Mach number effect (which effect has been analytically treated in refs. 6 and 7) is observed in the curve for the 4-inch body for $M_o = 0.801$ (fig. 11). Although thorough checking of the data revealed no errors, the entire level of the curve is thought low, and this curve should be regarded with suspicion. As the Mach number was increased from about 0.95 to 1.05, the pressure coefficients became more positive over much of the forebody. Above 1.05, the forebody pressure coefficients were not greatly affected by increase of the Mach number with the exception of the disturbances caused by the tunnel-wall reflected bow shocks. The bow-shock reflection (figs. 7 and 8) on to the model surface occurred sufficiently far downstream so that the forebody was nearly free of tunnel boundary interference at the highest test Mach number for the 8-inch body and, at Mach numbers above about 1.05, for the 4-inch body.

Effect of model size on pressure distribution.- Artificial constraint of the tunnel boundary at subsonic speeds and reflection of compression or expansion waves at supersonic speeds exert effects on a model which is dependent on the size of the model relative to the tunnel. The presence of such effects can be demonstrated by a comparison of the pressure distributions and force characteristics on geometrically similar models of different size. A comparison of the pressure distributions on the 8- and 4-inch bodies is given in figure 12.

The pressure distributions of figure 12 show a prominent tendency toward peaks at the same relative locations on both models (x/L values of about 0.3 and 0.45). The reason for this tendency is not explained by the contour measurements shown in figure 5, and visual inspection of the model failed to disclose any obvious causes of these peaks. There did seem to be a shallow ridge on the 8-inch body near the location of the front peak, and at the same relative location on the 4-inch body, a bump due to a slight separation of the Fiberglas laminae just off to the side of the orifice row. It does not seem likely that the tendency toward the formation of these bumps is inherent in the model design coordinates, since examination of these coordinates greatly expanded in the radial direction revealed no waves or flat spots.

At each of the subsonic Mach numbers, there are no significant differences in the shape of the curves for the two bodies. Although the

model surface irregularities may have been responsible for the considerable raggedness of the curves, a generally lower level of pressures appears to have been acting over the surface of the 8-inch body at $M_o \approx 0.6$. At $M_o \approx 0.95$, the forebody pressure distributions were closely alike, but the level of the pressure acting over the afterbody was again lower for the 8-inch model. There seem to be no important differences in the distributions of the two models for the Mach numbers of about 0.95 and 1.0.

At supersonic Mach numbers, the flow about the model becomes subject to the effects of tunnel-boundary-reflected compression and expansion waves. The nature of such reflections in a slotted test section is complex. Compression and expansion waves are reflected from the solid portions of the tunnel boundary as waves of the same kind. From the slots, however, the compressions are reflected as expansions, and the expansions, as compressions. The incidence of boundary-reflected compression waves on to the model surface is more easily observed than that of expansion waves because of the sharply localized nature of the compression disturbance. At the two highest test Mach numbers, the effects of the reflected bow shock are shown clearly on figure 12(c) as a strong local compression. This type of reflection appears to behave, qualitatively at least, as a reflection of the same type of shock incident on a solid boundary (figs. 7 and 8).

The prominent zone of higher pressure acting over the afterbody of the 8-inch model at Mach numbers of about 1.02 and 1.05 may possibly be associated with the region of the tunnel wall under the influence of the expanded flow about the region of the model near the maximum diameter station. The tunnel-wall Mach number distributions of figures 7(f) and 7(g) indicate that this region occurs at a location from which compressions would be transmitted to the afterbody if the region of expanded flow were reflected predominantly as a region of compression. At higher Mach numbers for the 8-inch model and at all of the supersonic Mach numbers for the 4-inch model, the region of expanded flow acting on the tunnel wall occurred too far downstream to transmit any such compressions to the model.

Drag measurements.- If, during the drag measurements of the two similar bodies, the extensive region of favorable pressure gradient on each body permitted the development of an extensive laminar boundary layer, differences in body Reynolds number and surface condition might have introduced drag changes which would tend to obscure the effects under study. Repeat runs were therefore made with transition strips (fig. 2). The boundary-layer thickness at the position of the transition strips, if laminar there, is estimated by the method of reference 8 as 0.017 inch and 0.013 inch for the 8- and 4-inch bodies, respectively. Since the average diameter of the carborundum grains (0.010 in.) is of the order of the boundary-layer thickness, it is presumed that no laminar boundary layer existed downstream from the transition strips.

The effect of the transition strips on the drag was small (fig. 13). It would seem, therefore, that the extent of laminar boundary layer on the models was small and that differences in the location of the transition point on the two bodies could not have introduced a spurious factor into the measurements. It should be noted that the 4- and 8-inch-model data are not comparable in figure 13 because of the presence of the tail cone and the absence of the cylindrical midsection during the transition strip runs of the 8-inch model (fig. 2).

Figure 14 presents the results of the drag measurements as obtained by the balance and by integration of the pressure distributions. A comparison of the pressure drag is also made with the balance drag reduced by the skin-friction drag which was estimated from the calculations of reference 9. This comparison shows good agreement for the 4-inch body, but it indicated a consistently high level for the pressure drag of the 8-inch body, which was obtained by an integration for the top row of pressure orifices. The pressure drag of the alternate model appears to be the more correct of the integrations for the two 8-inch bodies, but it is likewise consistently high. There is a certain amount of unreliability involved in the use of a single row of pressure orifices to measure the pressure drag, as indicated by figure 15. In addition to this possible source of error, the restricted number of pressure orifices and the poor surface condition of the afterbody may possibly account for this apparent discrepancy. For both bodies, however, the pressure drag by itself described the effects of Mach number on the body drag.

The effect of body size on the force and pressure drag is shown in figure 16. Throughout the subsonic Mach number range, the drag coefficients C_{D_e} are considered in good agreement in view of the accuracy of the measurement of this quantity and the difference in the friction drag of the two models. The accuracy of the force measurements was, of course, least at the lowest Mach number because of the low dynamic pressure. The effect of Mach number in the subsonic range was limited to the range above about 0.95, where a small, gradual rise occurred. The similarity of this drag rise for both bodies indicates the absence of any important subsonic boundary interference on the bodies.

At supersonic Mach numbers of about 1.02 and 1.05, large differences in the drag coefficients of the two bodies occurred as a result of the differences in the tunnel boundary effects. Although the drag coefficients of the two bodies were approximately equal at $M_o \approx 1.075$, both bodies were subject to strong interference from the tunnel boundary (figs. 7(h) and 8(h)). At the highest test Mach number, the 4-inch model was essentially free of tunnel boundary interference (fig. 8(h)) since the reflected bow shock passed downstream of the body. The agreement of the drag coefficients at this Mach number (fig. 16), however, does not mean that the 8-inch body was also free of interference.

Actually, the bow shock of this body was reflected from the tunnel boundary back to the model surface in the region near the body maximum diameter (fig. 7(i)). The effect of this reflection on the drag was small because the resultant region of increased pressure occurred in a region where the diameter was almost constant and also because it raised the pressure both upstream and downstream of the cylindrical midsection.

Three of the components of the body drag are presented in figure 17. Good agreement of the base drag coefficients is shown for the subsonic Mach numbers. The forebody- and afterbody-pressure-drag curves show that the transonic drag rise of the bodies investigated occurred almost entirely on the forebody. It is also shown that the forebody drag on both bodies was in fair agreement at Mach numbers up to about 1.05 in spite of the fact that both forebodies were subject to some boundary interference at Mach numbers from 1.0 to 1.05. At $M_0 \approx 1.05$ where this interference should be greatest, the forebody pressure drag of the 8-inch body agrees well with that of the 4-inch body, the forebody of which at this Mach number should be interference free (fig. 8(g)). Thus it might be correct to conclude that the boundary interference acting on the 8-inch forebody was small in this range of Mach number.

Drag measurements of fin-stabilized bodies in free flight usually indicate a sharp drag rise at subsonic speeds, a phenomenon which was not observed for the body shape of this investigation. Since tunnel interference was not believed to be a factor in this disagreement, it was presumed that the presence of the tail fins on the free-flight bodies are responsible. Figure 18 confirms this hypothesis. In the upper part of the figure are shown the drag curves for the 8-inch body and for this body fitted with cruciform delta tail fins. The increment between these two curves is the drag increment caused by the fins and their interference and is shown in the lower part of figure 18. This increment increased substantially between a Mach number of about 0.91 and 1.0 from where it tended to diminish as the Mach number was increased. Most of the subsonic rise of this increment must be due to the interference of the fins since the fins and the body individually have only small subsonic drag rises.

CONCLUDING REMARKS

The following remarks summarize the principal results of an investigation of some factors affecting the drag of two geometrically similar nonlifting bodies of revolution of 8- and 4-inch maximum diameter in the slotted Langley 8-foot transonic tunnel.

Drag and pressure measurements confirmed a result of a prior investigation which had indicated that no important tunnel boundary interference should occur on the bodies at subsonic Mach numbers.

A disagreement between the character of the observed subsonic drag rise and that usually observed for fin-stabilized bodies in free flight was shown to be the result of fin interference.

Large effects of tunnel-boundary reflected disturbances on the drag were found at some supersonic Mach numbers. Although a strong compression reflection acted on the larger body at the highest test Mach number of approximately 1.12, the resultant interference was such that the drag coefficient of this body was approximately equal to that of the smaller body, which was essentially free of tunnel interference at this Mach number.

The forebody was nearly free of tunnel interference at the highest test Mach number for the larger body (approx. 1.12) and, at Mach numbers greater than about 1.05 for the smaller body. At Mach numbers above these values and below the Mach number at which the bow shock was reflected to the region downstream from the model base, tunnel interference on the drag resulted from interference on the afterbody.

Langley Aeronautical Laboratory,
National Advisory Committee for Aeronautics,
Langley Field, Va.

REFERENCES

1. Wright, Ray H., and Ritchie, Virgil S.: Characteristics of a Transonic Test Section With Various Slot Shapes in the Langley 8-Foot High-Speed Tunnel. NACA RM L51H10, 1951.

2. Wright, Ray H., and Ward, Vernon G.: NACA Transonic Wind-Tunnel Test Sections. NACA RM L8J06, 1948.

3. Ritchie, Virgil S., and Pearson, Albin O.: Calibration of the Slotted Test Section of the Langley 8-Foot Transonic Tunnel and Preliminary Experimental Investigation of Boundary-Reflected Disturbances. NACA RM L51K14, 1952.

4. Sears, Richard I., and Merlet, C. F.: Flight Determination of the Drag and Pressure Recovery of an NACA 1-40-250 Nose Inlet at Mach Numbers From 0.9 to 1.8. NACA RM L50L18, 1951.

5. Thompson, Jim Rogers: Measurements of the Drag and Pressure Distribution on a Body of Revolution Throughout Transition From Subsonic to Supersonic Speeds. NACA RM L9J27, 1950.

6. Ackeret, J.: Über Luftkräfte bei sehr grossen Geschwindigkeiten insbesondere bei ebenen Strömungen. Helvetica Physica Acta, vol. I, fasc. 5, 1928, pp. 301-322.

7. Von Kármán, Th.: Compressibility Effects in Aerodynamics. Jour. Aero. Sci., vol. 8, no. 9, July 1941, pp. 337-356.

8. Jacobs, E. N., and Von Doenhoff, A. E.: Formulas for Use in Boundary-Layer Calculations on Low-Drag Wings. NACA ACR, Aug. 1941.

9. Young, A. D.: The Calculation of the Total and Skin Friction Drags of Bodies of Revolution at Zero Incidence. R. & M. No. 1874, British A.R.C., 1939.

TABLE I

DESIGN AND MEASURED FUSELAGE COORDINATES

Design coordinates				Measured coordinates			
8-inch model		4-inch model		8-inch model		4-inch model	
x	r	x	r	x	r	x	r
0	0	0	0	1.504	0.671	1.468	0.559
.320	.222	.160	.111	2.004	.828	1.718	.628
.480	.286	.240	.143	2.504	.970	1.968	.685
.800	.411	.400	.206	3.004	1.110	2.218	.744
1.600	.693	.800	.347	3.504	1.242	2.468	.800
2.750	1.033	1.375	.517	4.004	1.368	2.718	.852
3.200	1.157	1.875	.649	4.504	1.490	2.968	.907
3.250	1.171	2.400	.775	5.004	1.606	3.218	.956
3.500	1.235	3.200	.946	5.504	1.718	3.468	1.009
3.750	1.298	3.750	1.053	6.004	1.823	3.718	1.052
4.800	1.549	4.800	1.245	6.504	1.926	3.968	1.099
6.400	1.892	6.250	1.464	7.004	2.025	4.218	1.145
7.500	2.106	6.400	1.483	7.504	2.122	4.468	1.189
7.750	2.155	8.000	1.663	8.004	2.215	4.718	1.233
9.600	2.489	8.625	1.721	8.504	2.305	4.968	1.273
12.500	2.927	9.600	1.796	9.004	2.393	5.218	1.315
12.750	2.960	10.250	1.837	9.504	2.476	5.468	1.353
12.800	2.966	11.200	1.888	10.004	2.560	5.718	1.389
16.000	3.326	12.250	1.930	10.504	2.640	5.968	1.424
17.000	3.419	12.800	1.951	11.004	2.716	6.218	1.457
17.250	3.442	14.250	1.991	11.504	2.787	6.468	1.489
17.500	3.461	14.400	1.994	12.004	2.860	6.718	1.521
17.750	3.482	15.000	2.000	12.504	2.930	6.968	1.549
19.200	3.591	16.000	2.000	13.004	2.992	7.218	1.579
20.500	3.674	17.250	2.000	13.504	3.055	7.468	1.612
20.750	3.689	20.050	1.982	14.004	3.115	7.718	1.640
22.400	3.776	22.850	1.932	14.504	3.173	7.968	1.663
24.500	3.860	25.650	1.844	15.004	3.230	8.218	1.687
24.750	3.870	28.450	1.710	15.504	3.280	8.468	1.713
25.600	3.901	31.250	1.502	16.004	3.330	8.718	1.733
28.500	3.981	33.250	1.300	16.504	3.375	8.968	1.752
28.750	3.986			17.004	3.422	9.218	1.770
28.800	3.987			17.504	3.465	9.468	1.788
30.000	4.000			18.004	3.503	9.718	1.802
32.000	4.000			18.504	3.544	9.968	1.818
37.600	3.964			19.004	3.578	9.986	1.819
43.200	3.863			19.504	3.616	10.218	1.831
48.800	3.688			20.004	3.648	10.718	1.852
54.400	3.419			21.004	3.702	11.218	1.884
60.000	3.003			22.004	3.754	11.718	1.909
64.000	2.600			23.004	3.800	12.218	1.931
				24.004	3.841	12.718	1.948
				25.004	3.880	13.218	1.967
				26.004	3.918	13.718	1.973
				27.004	3.948	14.218	1.983
				28.004	3.974	14.618	1.989
				29.004	3.990	14.818	1.989
				30.004	3.998	15.718	1.987
				31.004	3.998	16.718	1.978
				32.004	3.998	17.718	1.977
						18.718	1.971
						19.718	1.960
						20.718	1.947
						21.718	1.932
						22.718	1.910
						23.718	1.883
						24.718	1.851
						25.718	1.817
						26.718	1.777
						27.718	1.272
						28.718	1.663
						29.718	1.590
						30.718	1.511
						31.718	1.426
						32.718	1.327
						33.152	1.271

NACA

TABLE II

MEASURED ORIFICE LOCATIONS

8-inch model		4-inch model	
x	r	x	r
0	0	0.543	0.278
1.003	.498	1.524	.566
2.004	.815	2.463	.787
3.004	1.103	3.456	1.012
4.004	1.365	4.464	1.207
5.003	1.604	5.488	1.352
6.004	1.821	6.452	1.493
7.004	2.017	7.452	1.616
8.003	2.205	8.453	1.716
9.004	2.388	9.454	1.793
10.002	2.555	10.449	1.846
11.001	2.705	11.455	1.896
11.996	2.850	12.446	1.946
12.984	2.938	13.428	1.974
13.998	3.111	14.484	1.988
14.983	3.222	15.314	1.990
15.993	3.323	15.952	1.990
16.994	3.420	16.548	1.990
18.004	3.500	17.119	1.990
18.998	3.573	18.461	1.986
19.994	3.639	21.368	1.946
21.002	3.696	22.792	1.918
22.001	3.746	25.277	1.844
23.001	3.789	26.160	1.766
24.004	3.839	30.092	1.571
25.002	3.878	31.559	1.469
26.000	3.913	32.834	1.320
26.999	3.946		
28.003	3.971		
29.004	3.987		
29.997	3.994		
30.746	3.997		
32.746	4.000		
36.522	3.994		
39.426	3.966		
42.325	3.918		
45.220	3.863		
53.918	3.567		
59.731	3.180		
65.504	2.658		

NACA

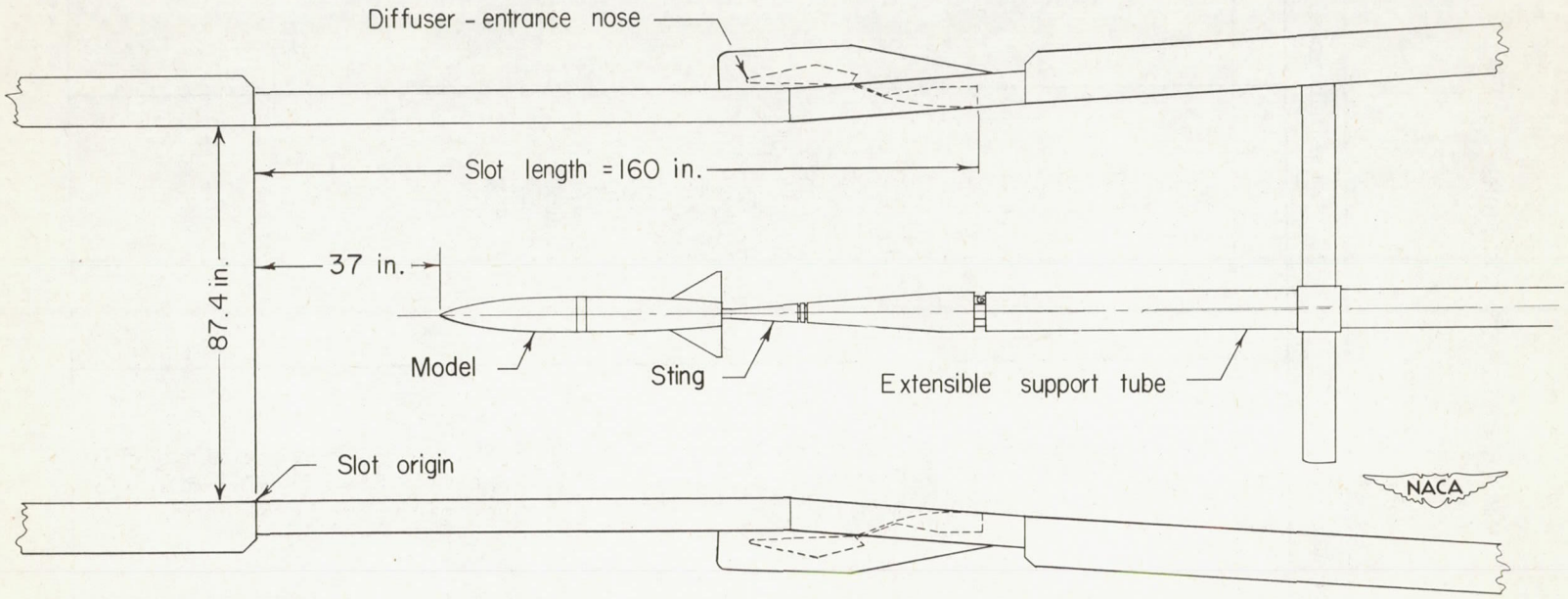

Figure 1.- Model on support in tunnel.

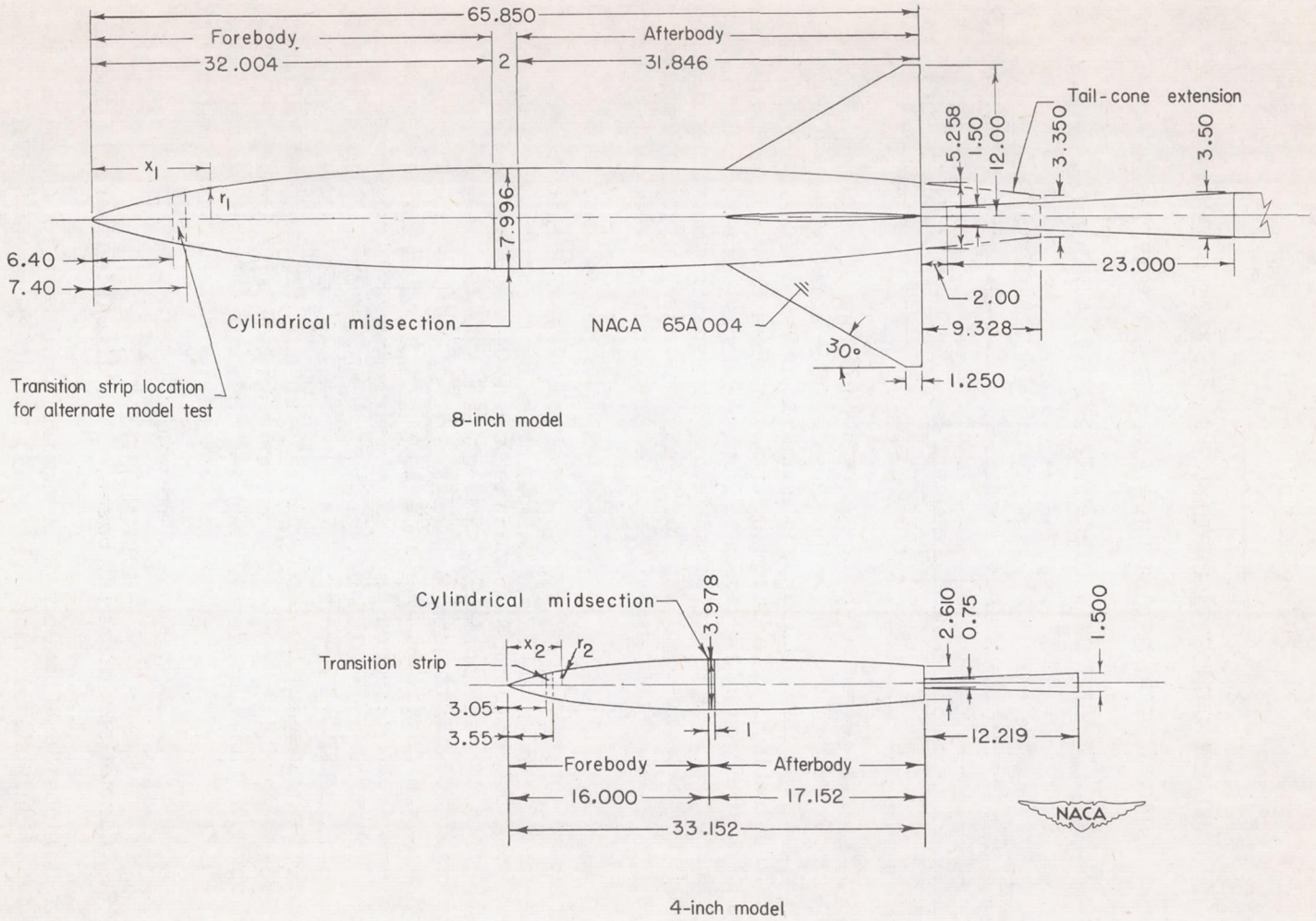

Figure 2.- Model dimensions. All dimensions are in inches.

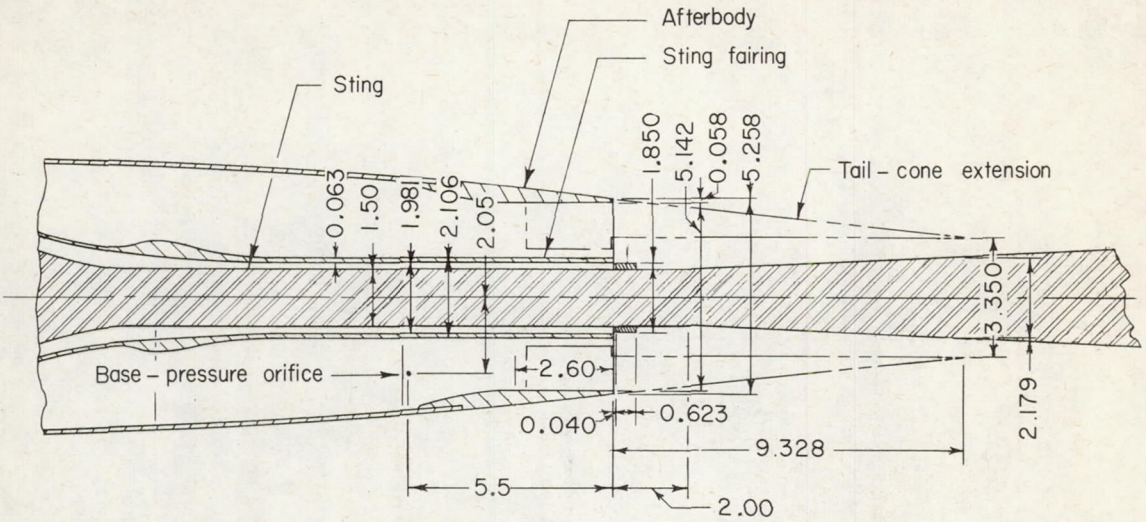

8-inch model

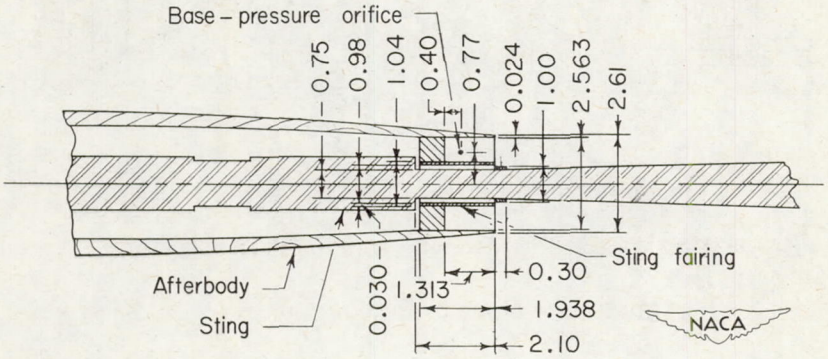

4-inch model

Figure 3.- Comparison of model bases. All dimensions are in inches.

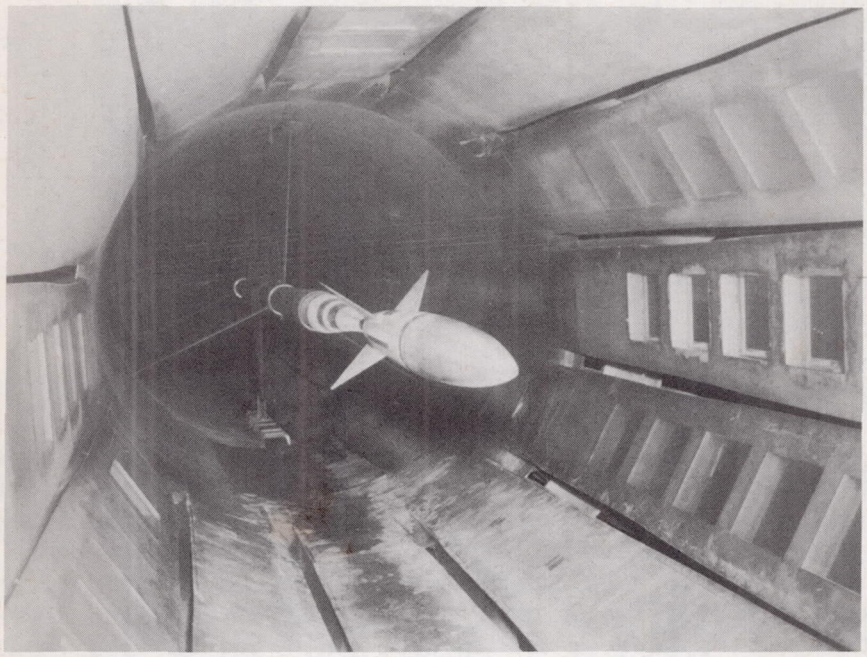

NACA
L-72806

(a) 8-inch finned model as mounted in tunnel.

Figure 4.- Model photographs.

L-74618

(b) 4-inch model and sting and 8-inch-model forebody.

Figure 4.- Concluded.

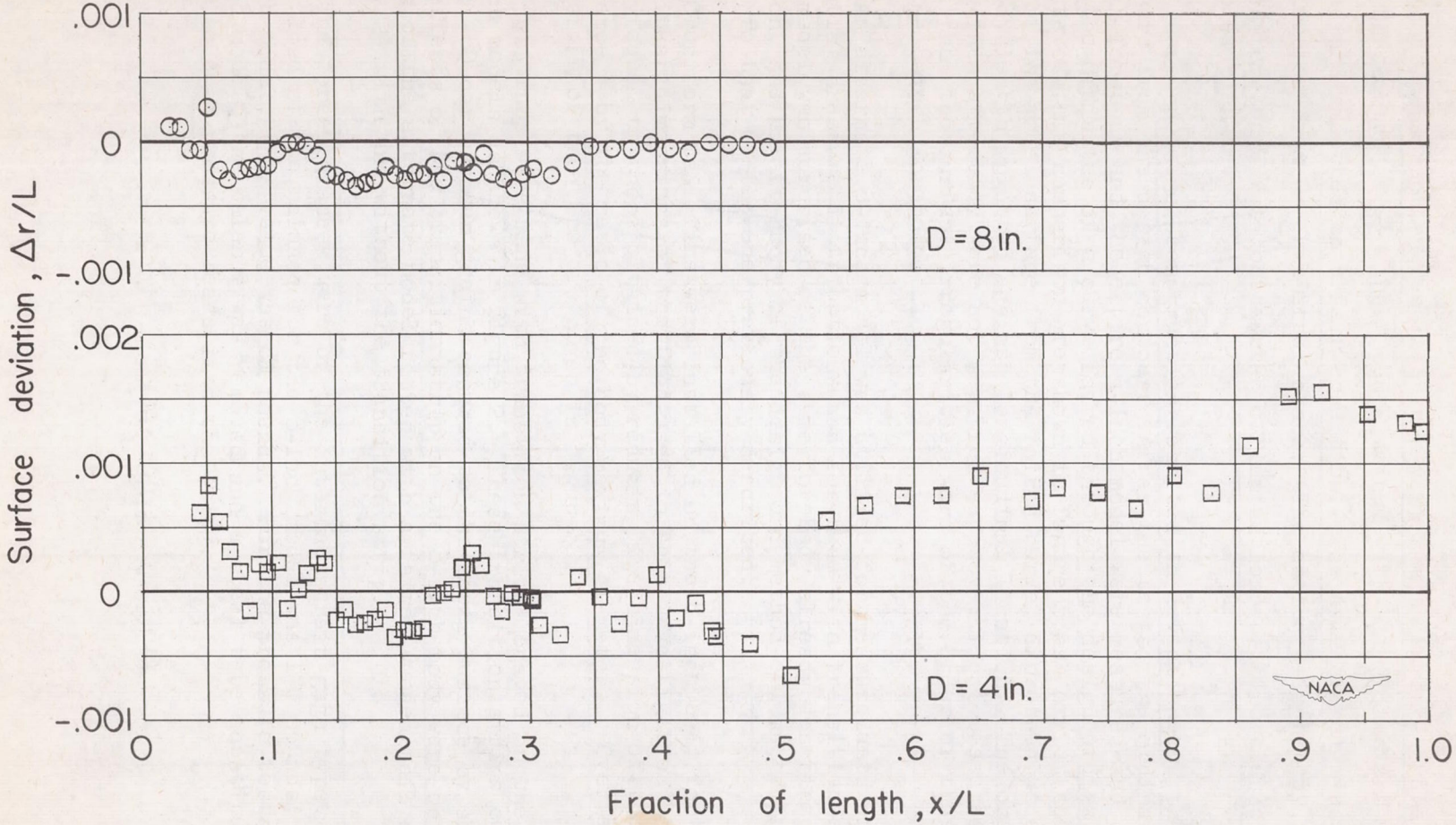

Figure 5.- Deviation of body surface contours from design contours.

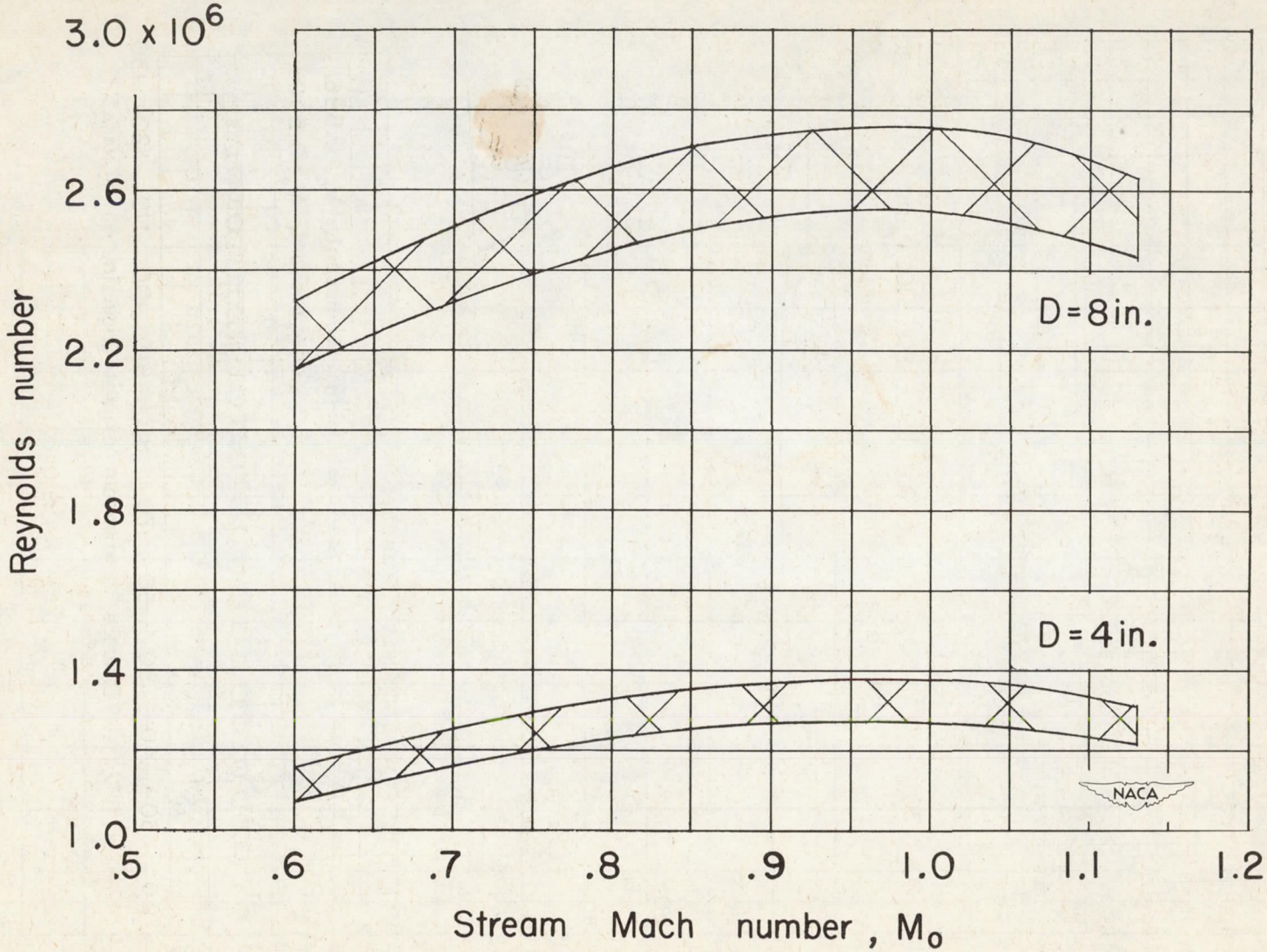

Figure 6.- Test Reynolds number range based on model maximum diameter.

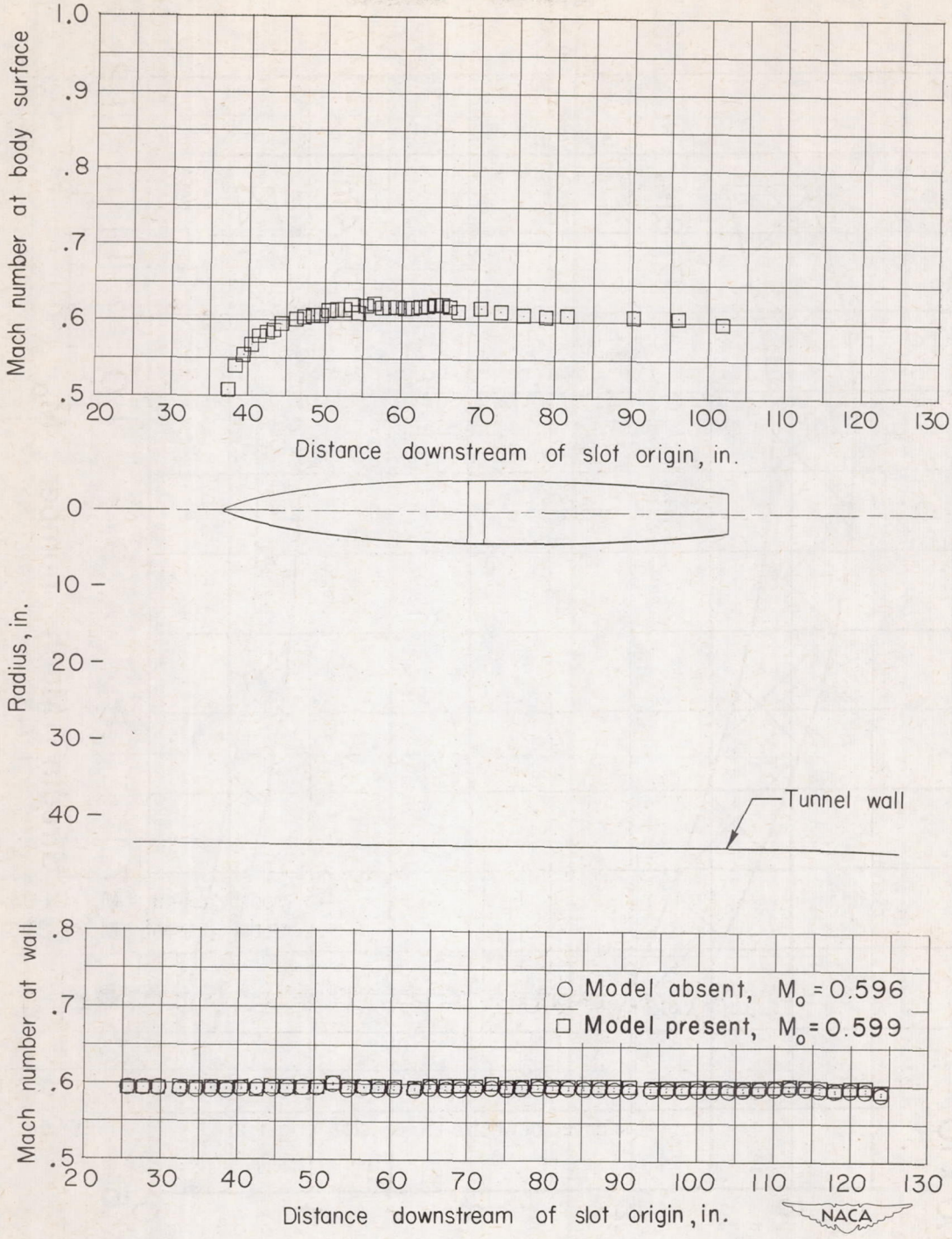

(a) $M_o \approx 0.60$.

Figure 7.- Model-surface and tunnel-wall Mach number distributions. D = 8 inches.

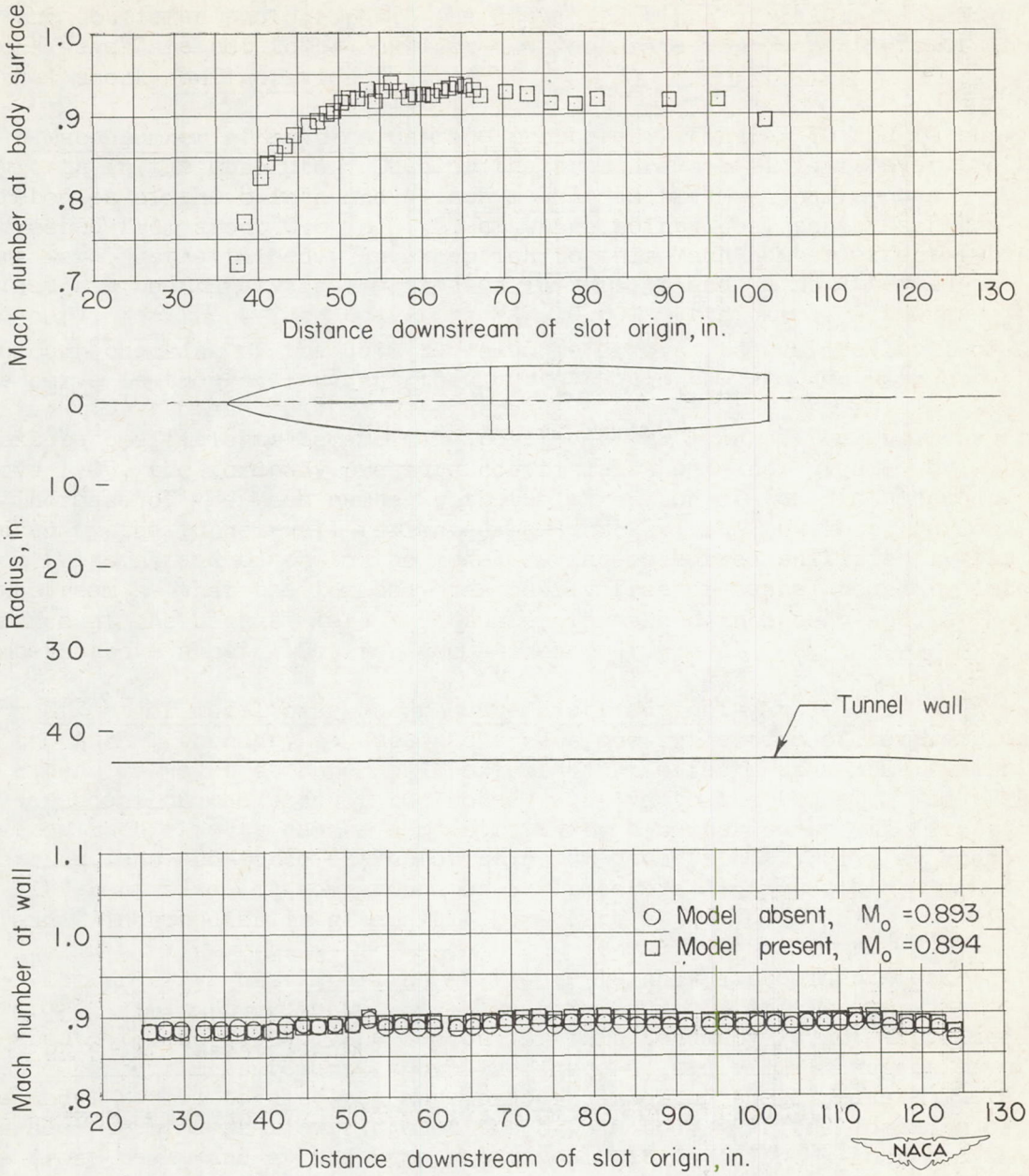

(b) $M_o \approx 0.90$.

Figure 7.- Continued.

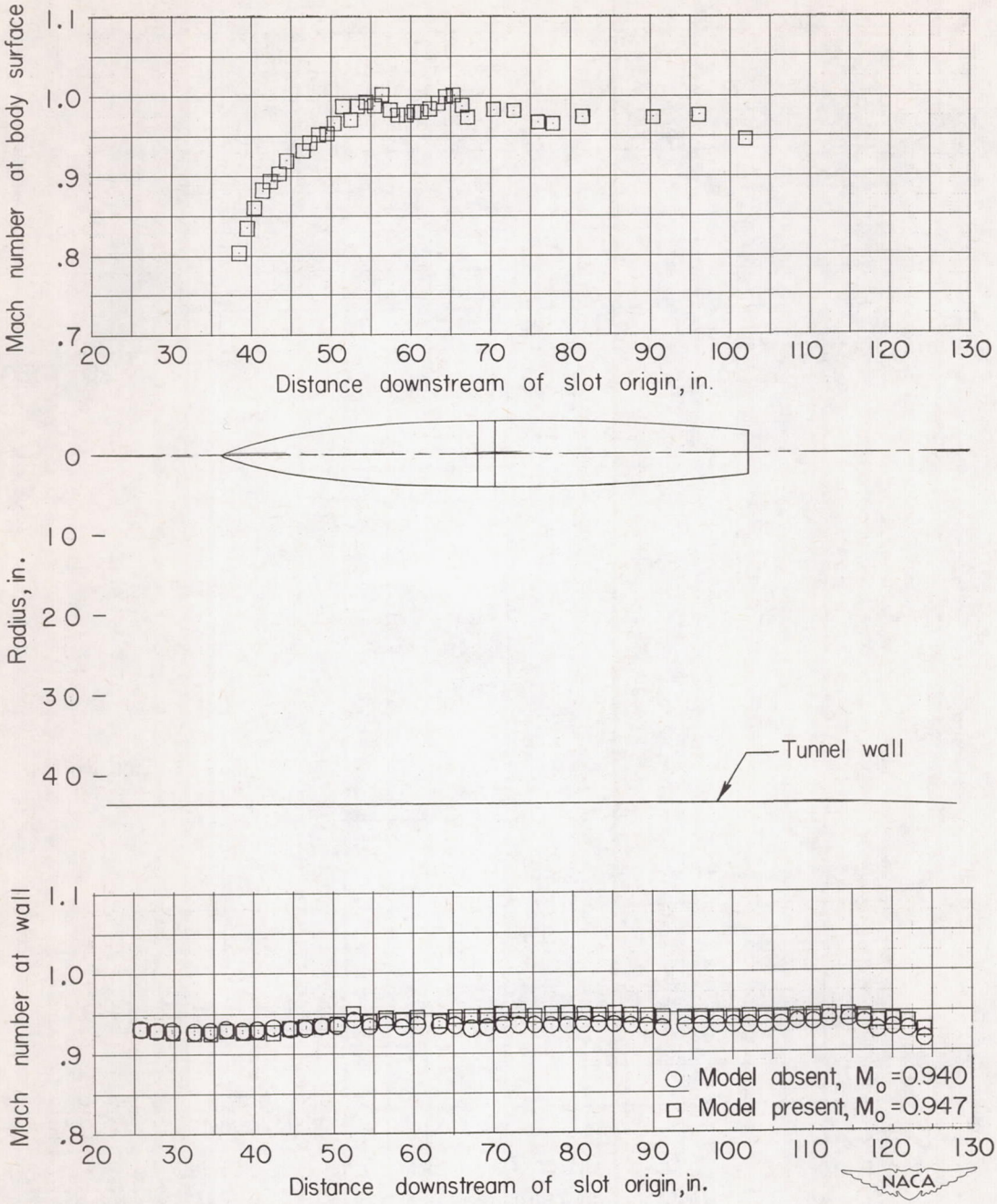

(c) $M_0 \approx 0.95$.

Figure 7.- Continued.

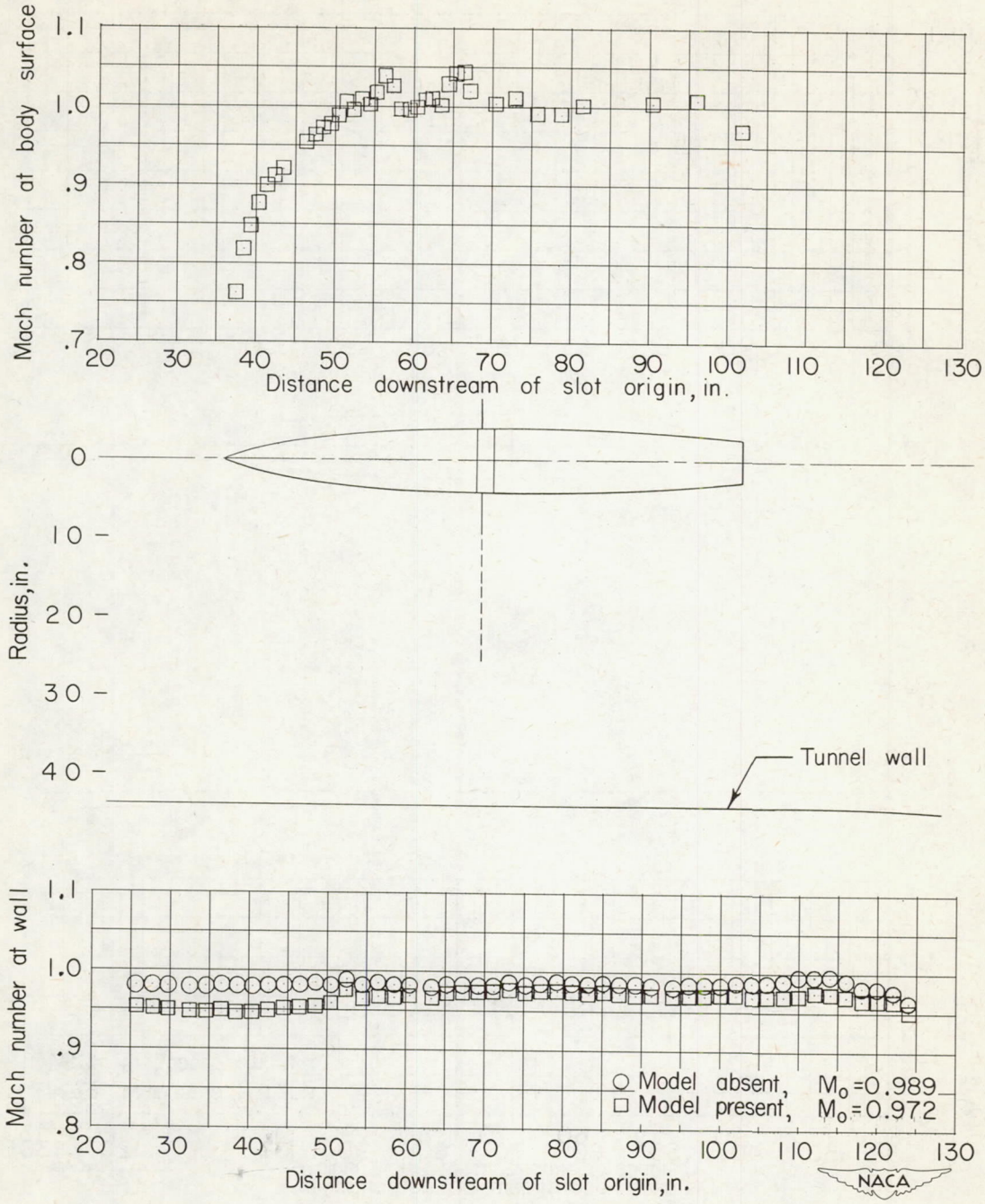

(d) $M_o \approx 0.975$.

Figure 7.- Continued.

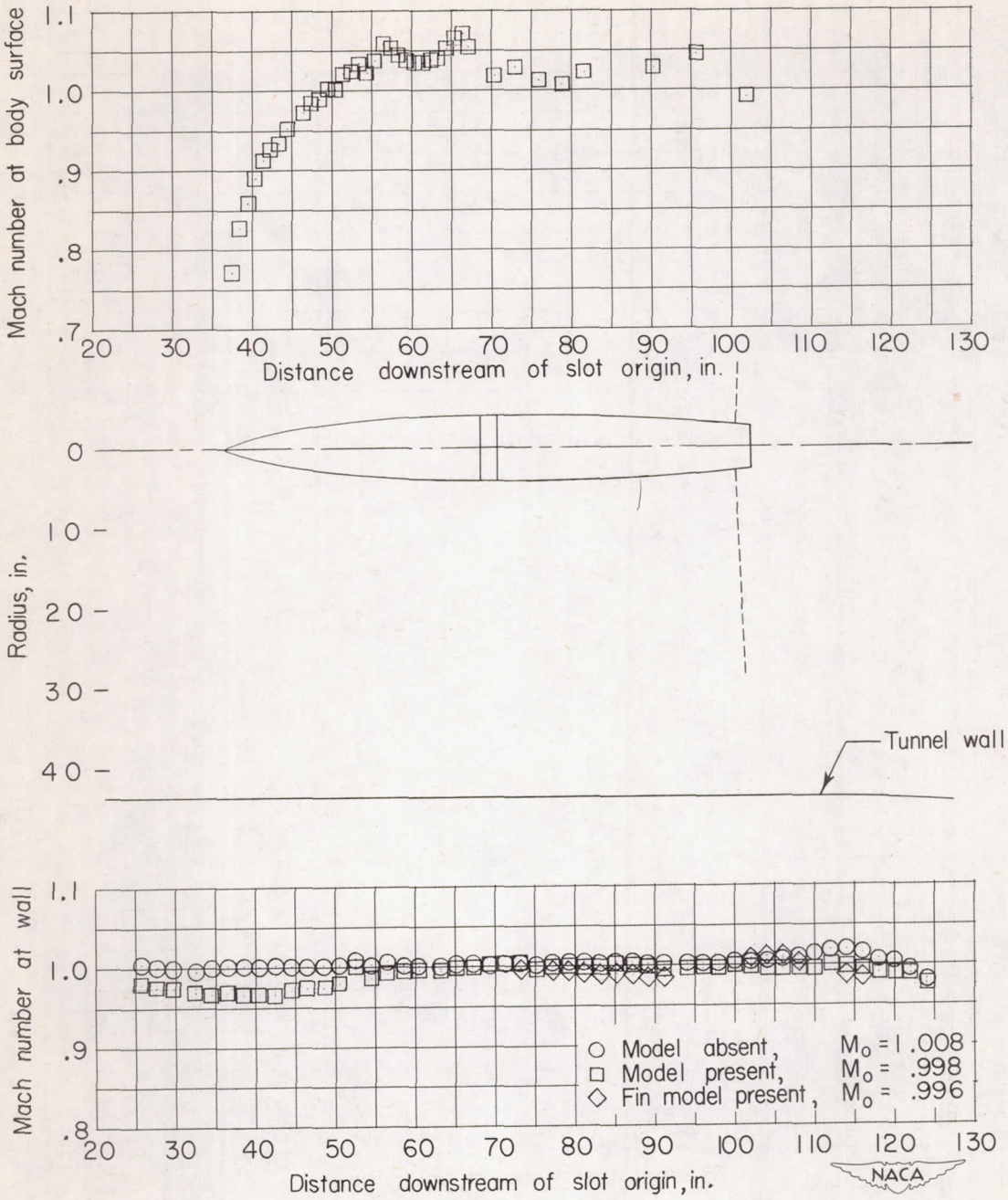

(e) $M_o \approx 1.00$.

Figure 7.- Continued.

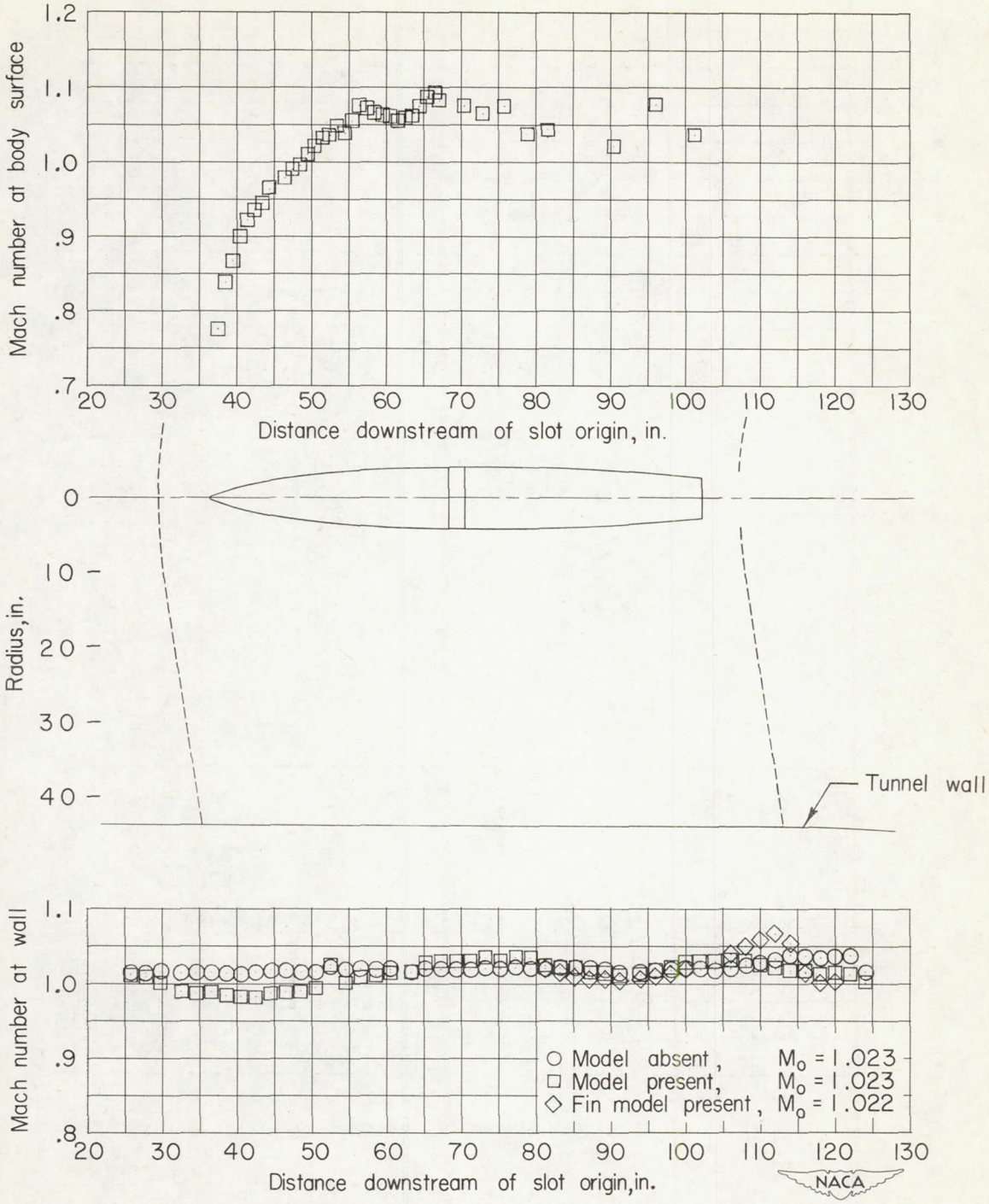

(f) $M_o \approx 1.025$.

Figure 7.- Continued.

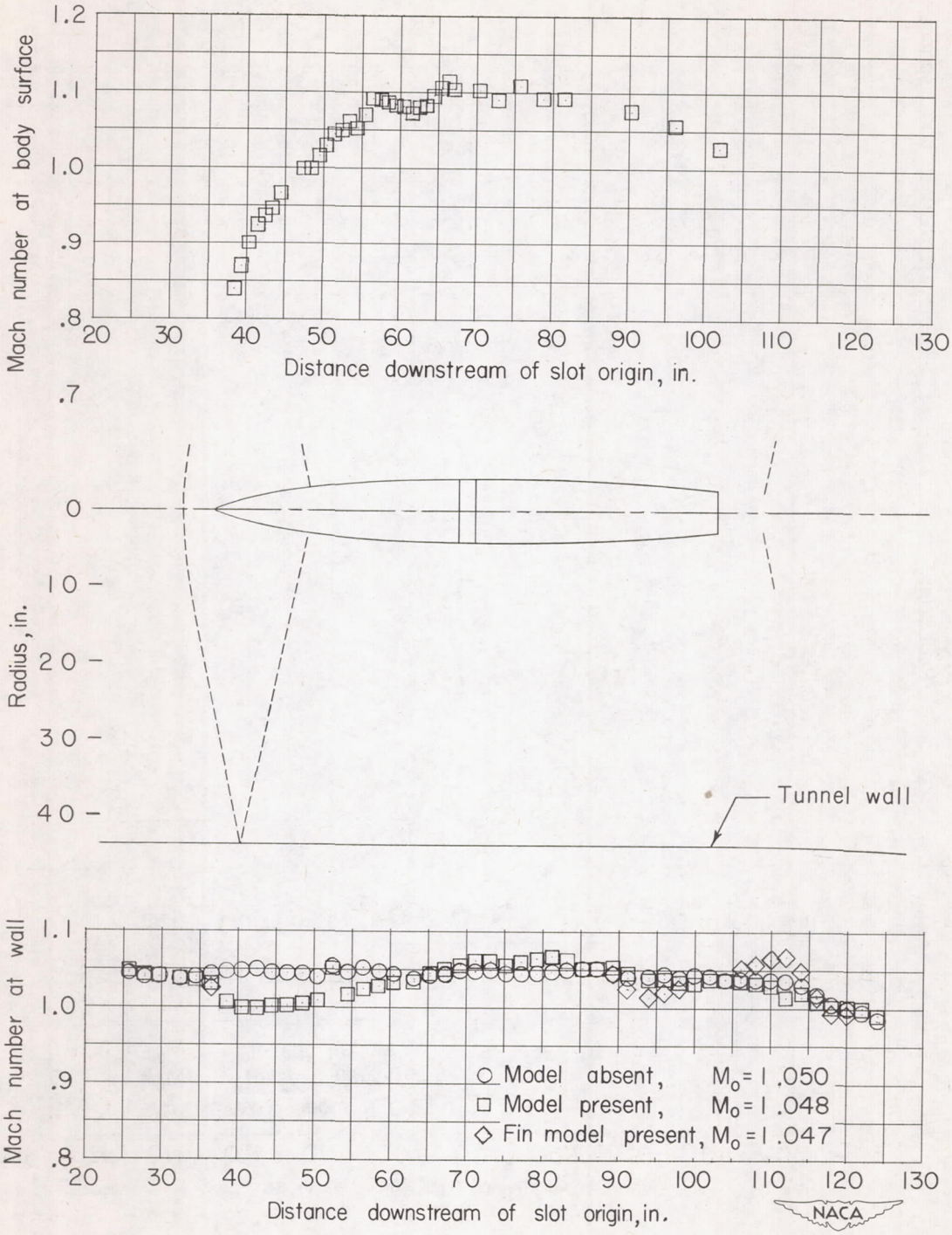

(g) $M_0 \approx 1.05$.

Figure 7.- Continued.

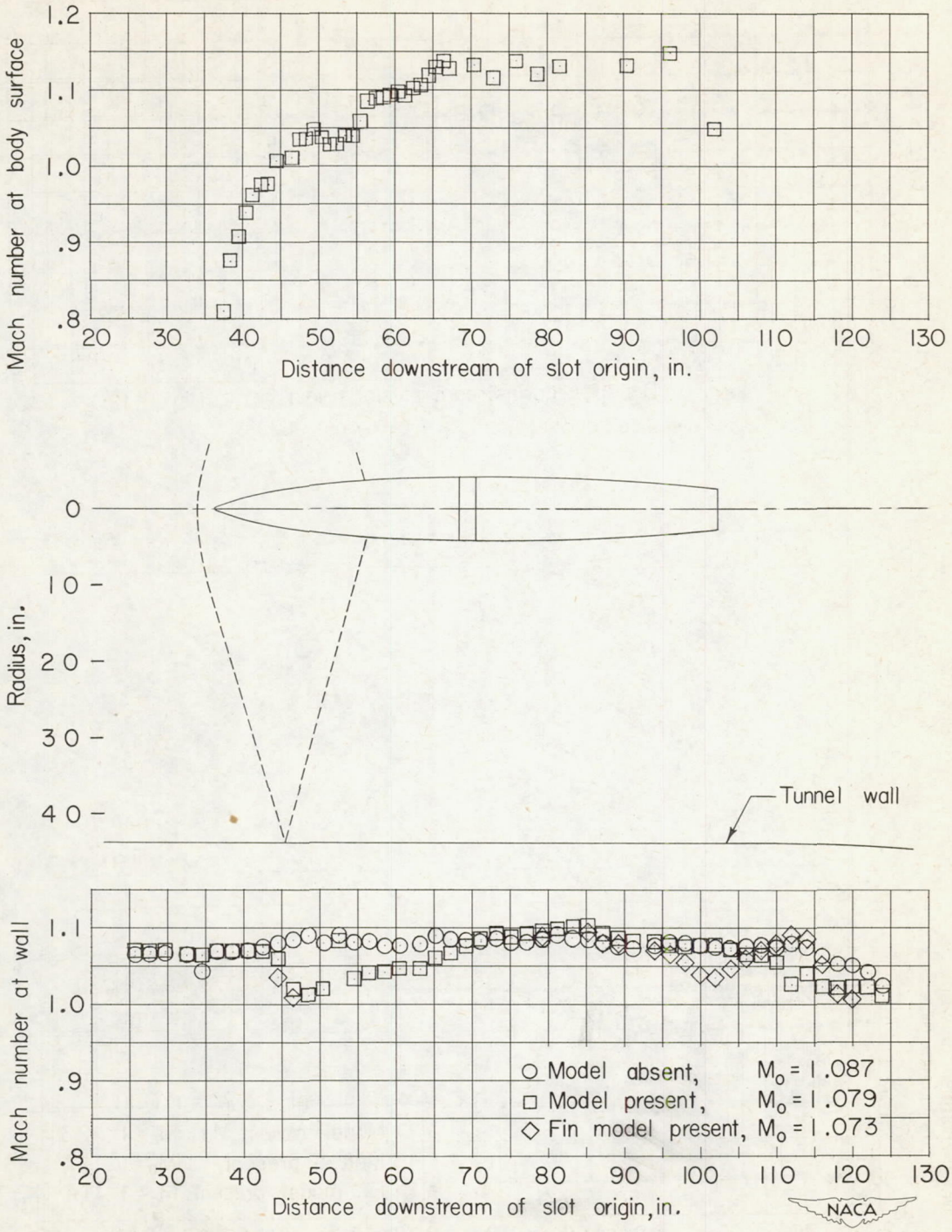

(h) $M_o \approx 1.08$.

Figure 7.- Continued.

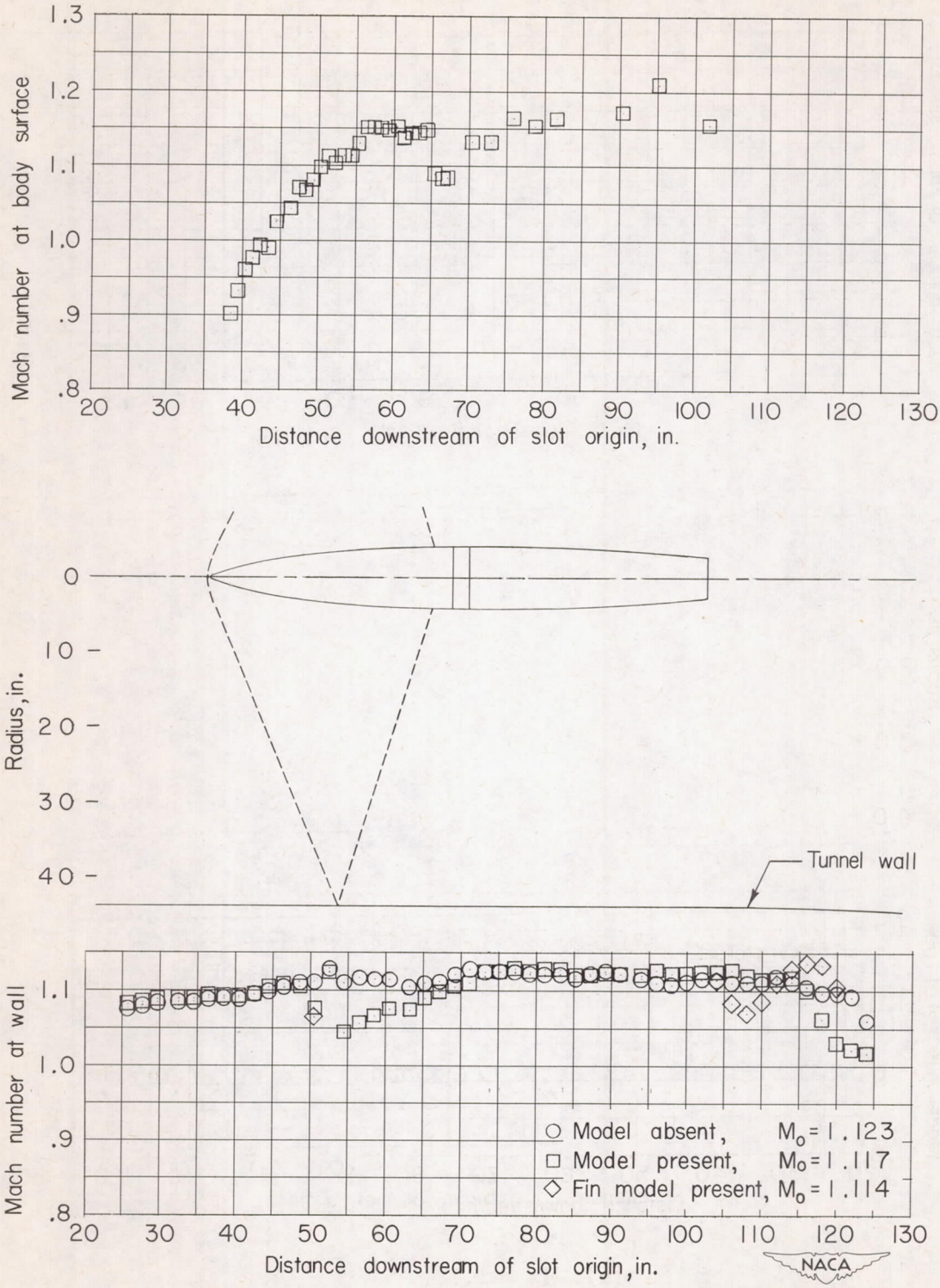

(i) $M_o \approx 1.12$.

Figure 7.- Concluded.

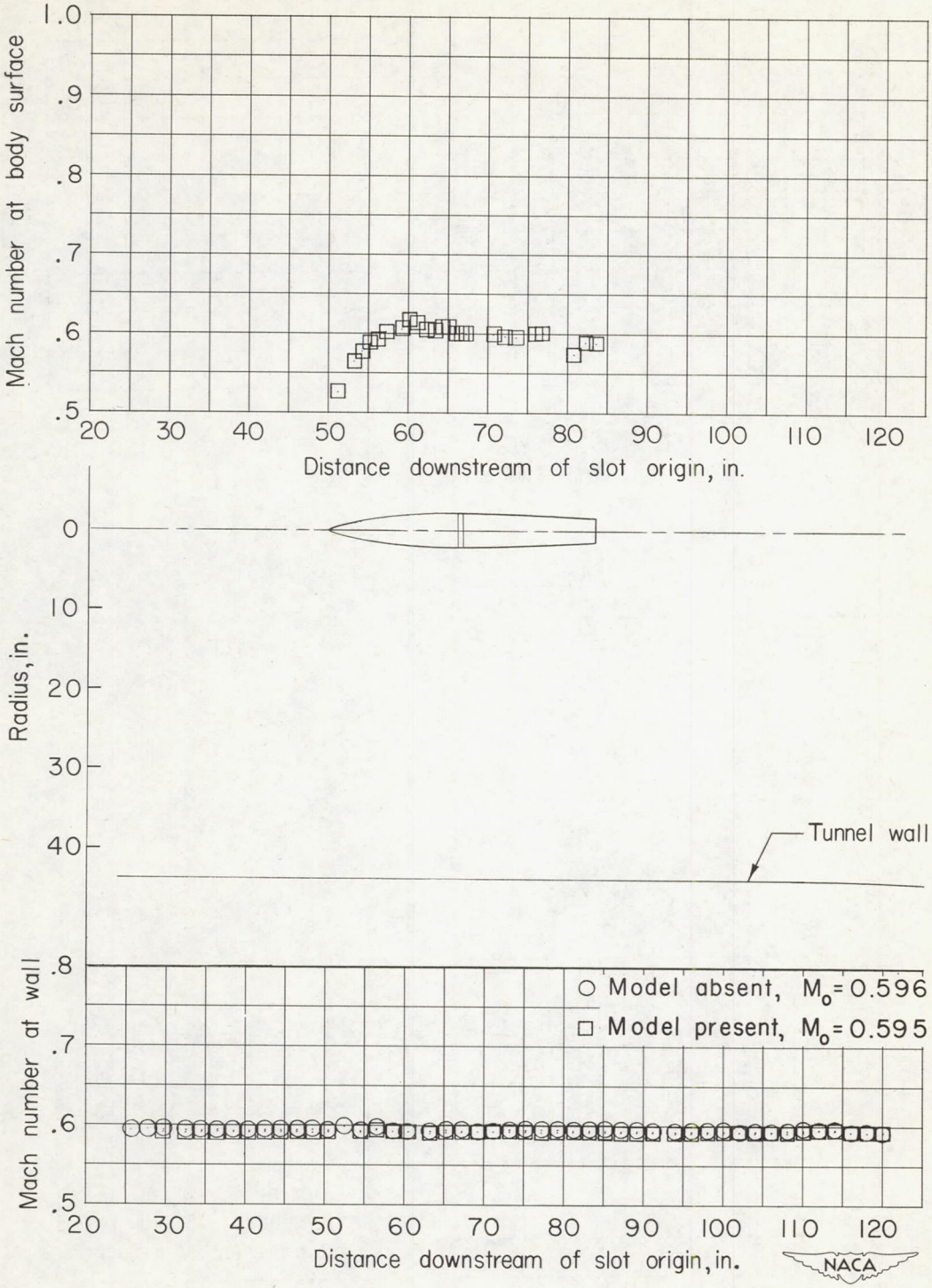

(a) $M_o \approx 0.60$.

Figure 8.- Model-surface and tunnel-wall Mach number distributions. D = 4 inches.

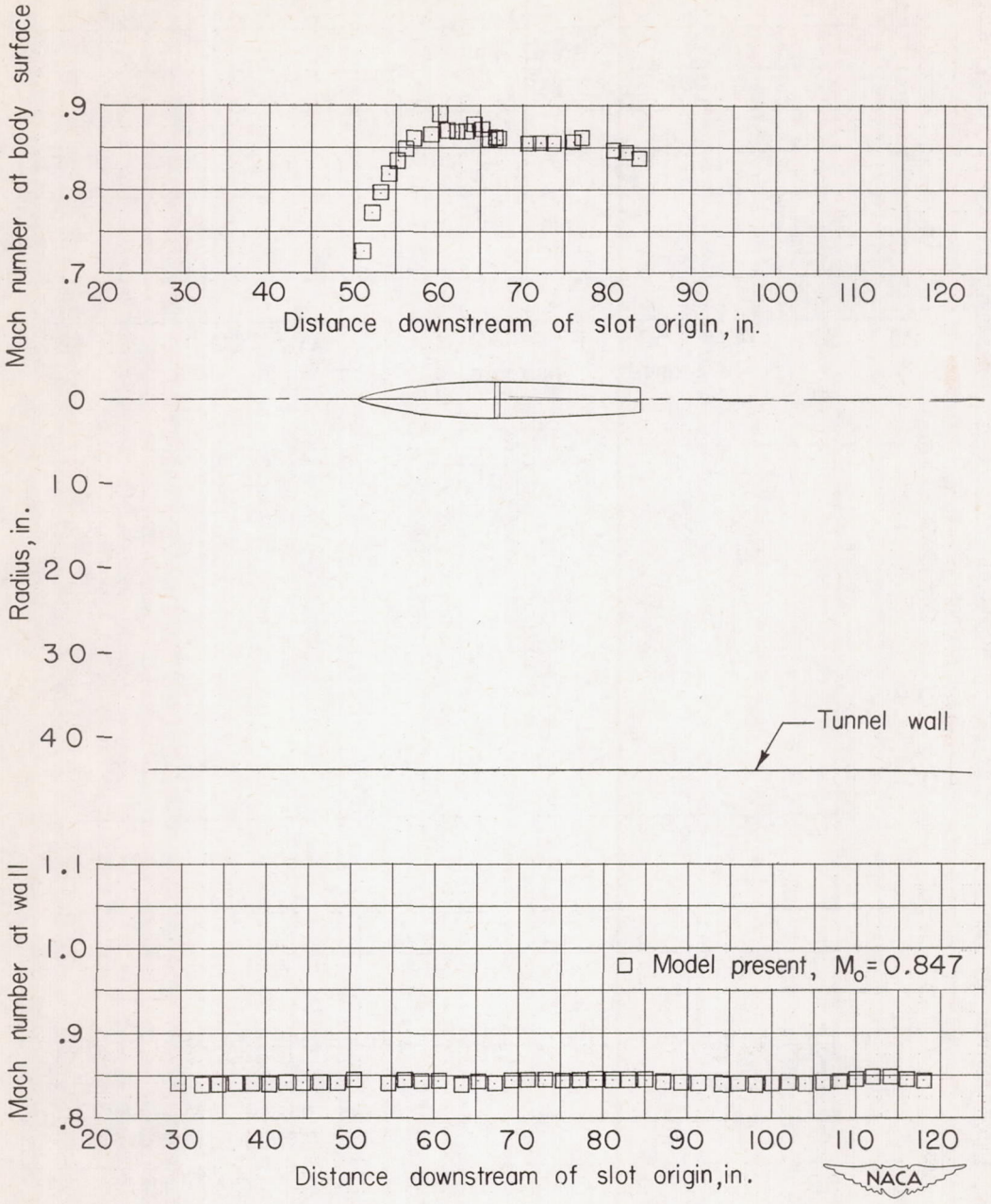

(b) $M_o \approx 0.85$.

Figure 8.- Continued.

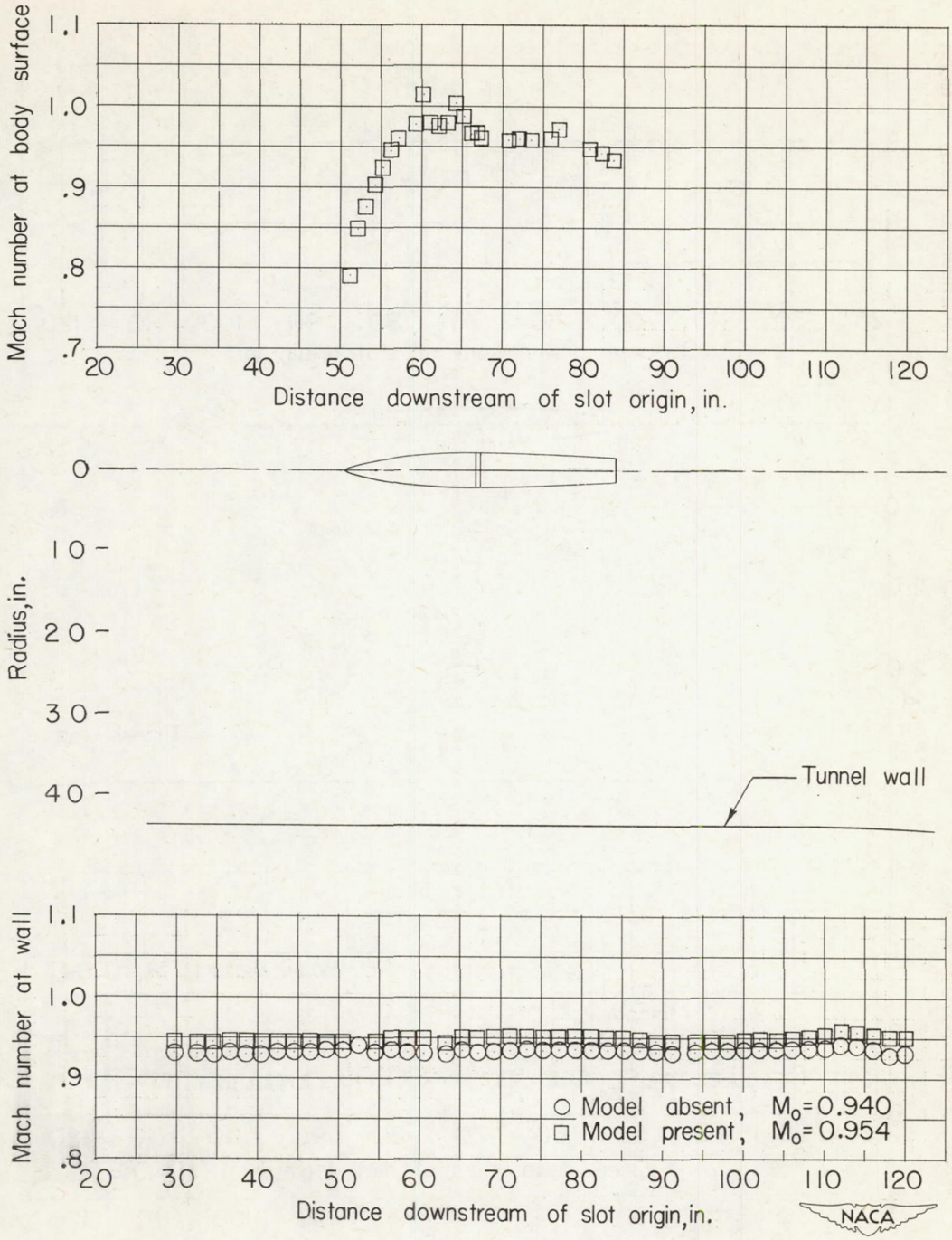

(c) $M_o \approx 0.95$.

Figure 8.- Continued.

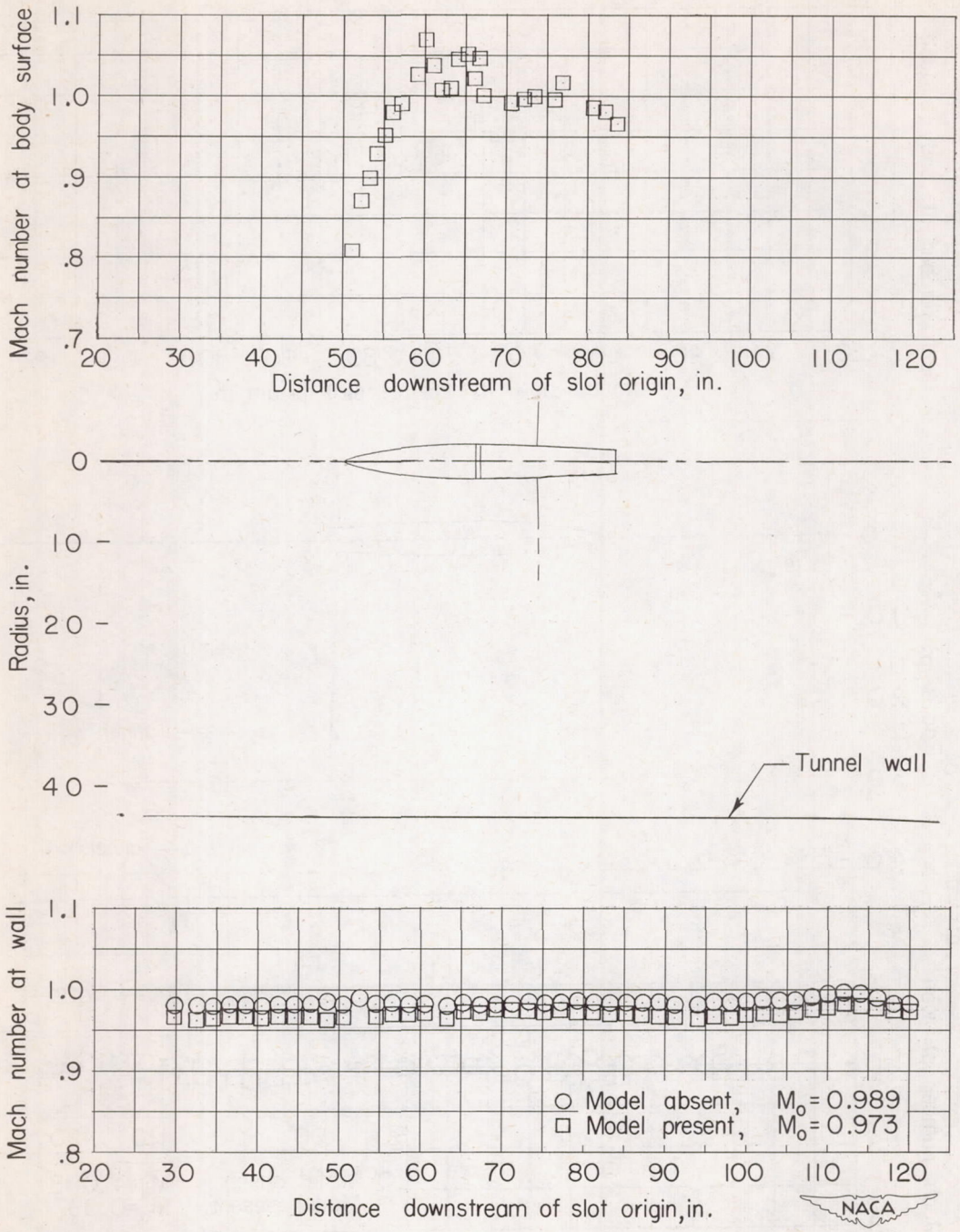

(d) $M_o \approx 0.975$.

Figure 8.- Continued.

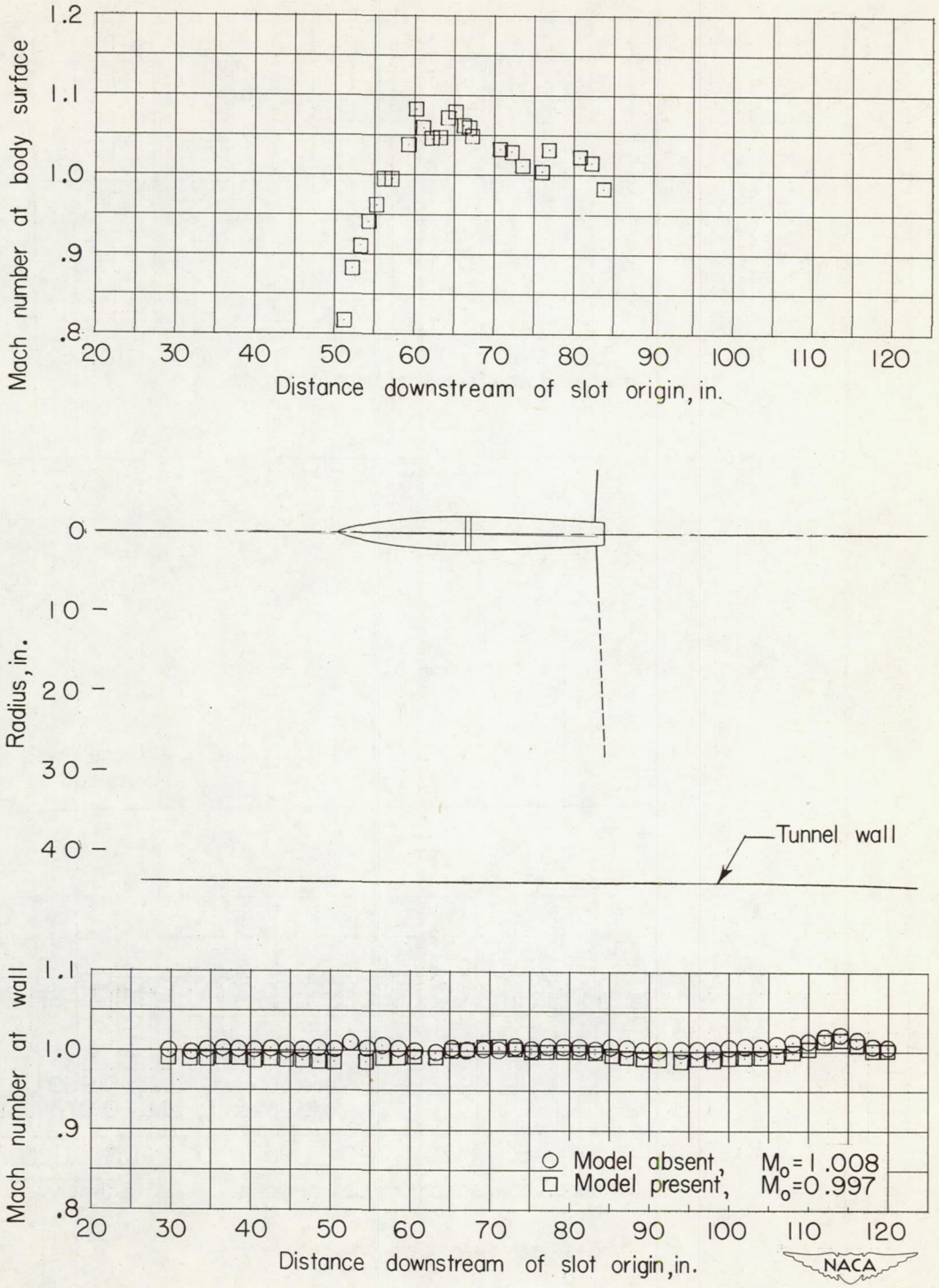

(e) $M_o \approx 1.00$.

Figure 8.- Continued.

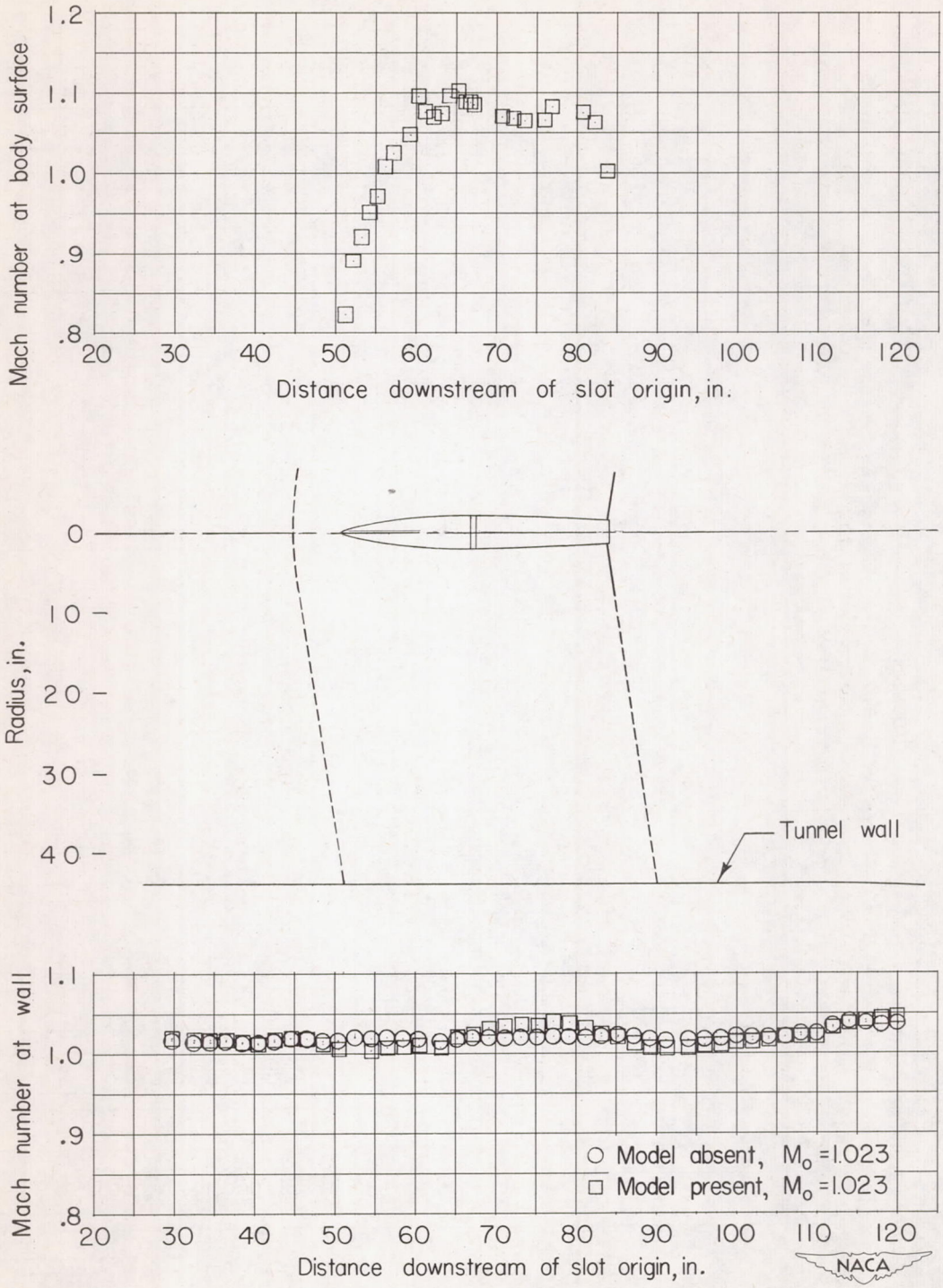

(f) $M_o \approx 1.025$.

Figure 8.- Continued.

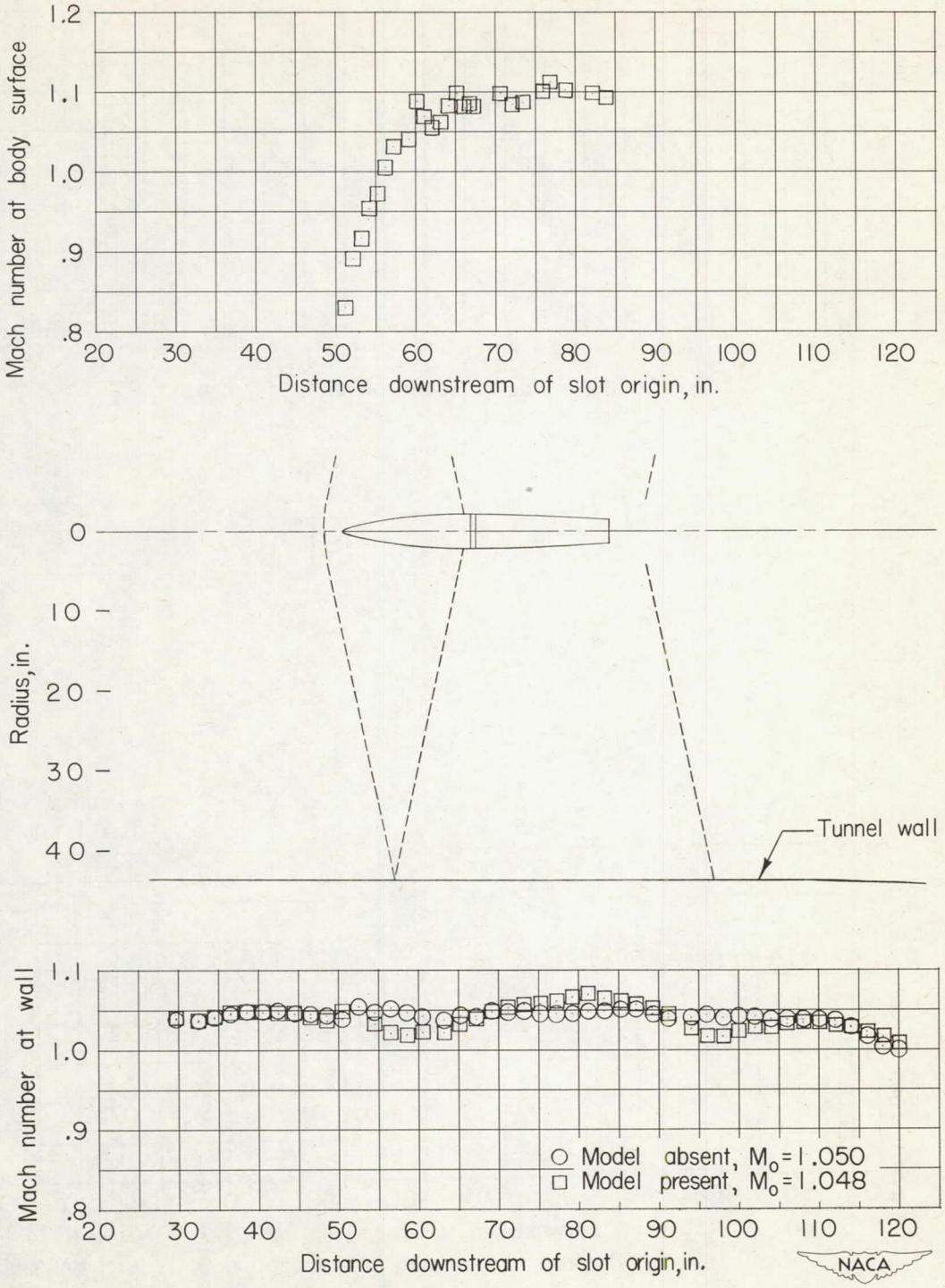

(g) $M_o \approx 1.05$.

Figure 8.- Continued.

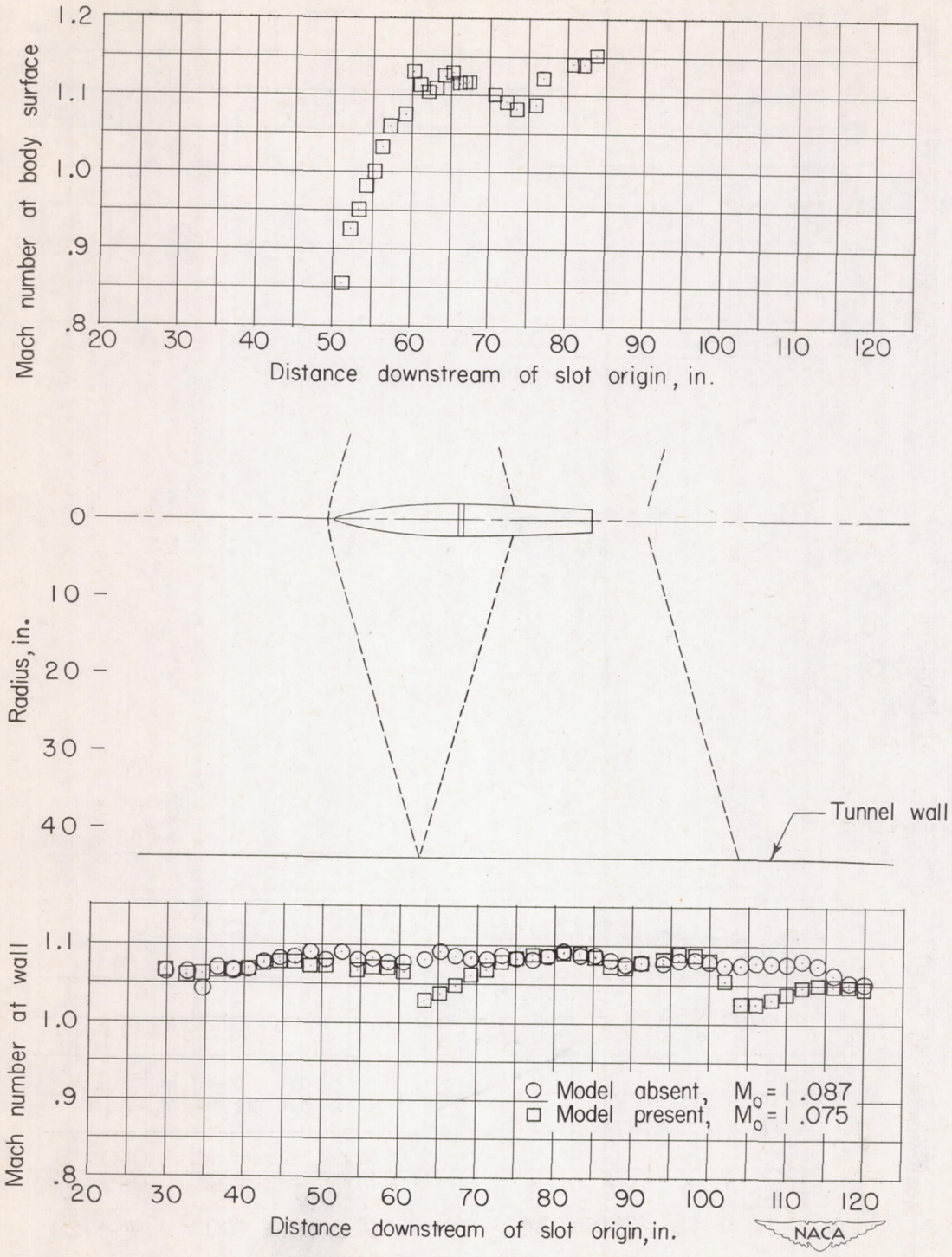

(h) $M_o \approx 1.075$.

Figure 8.- Continued.

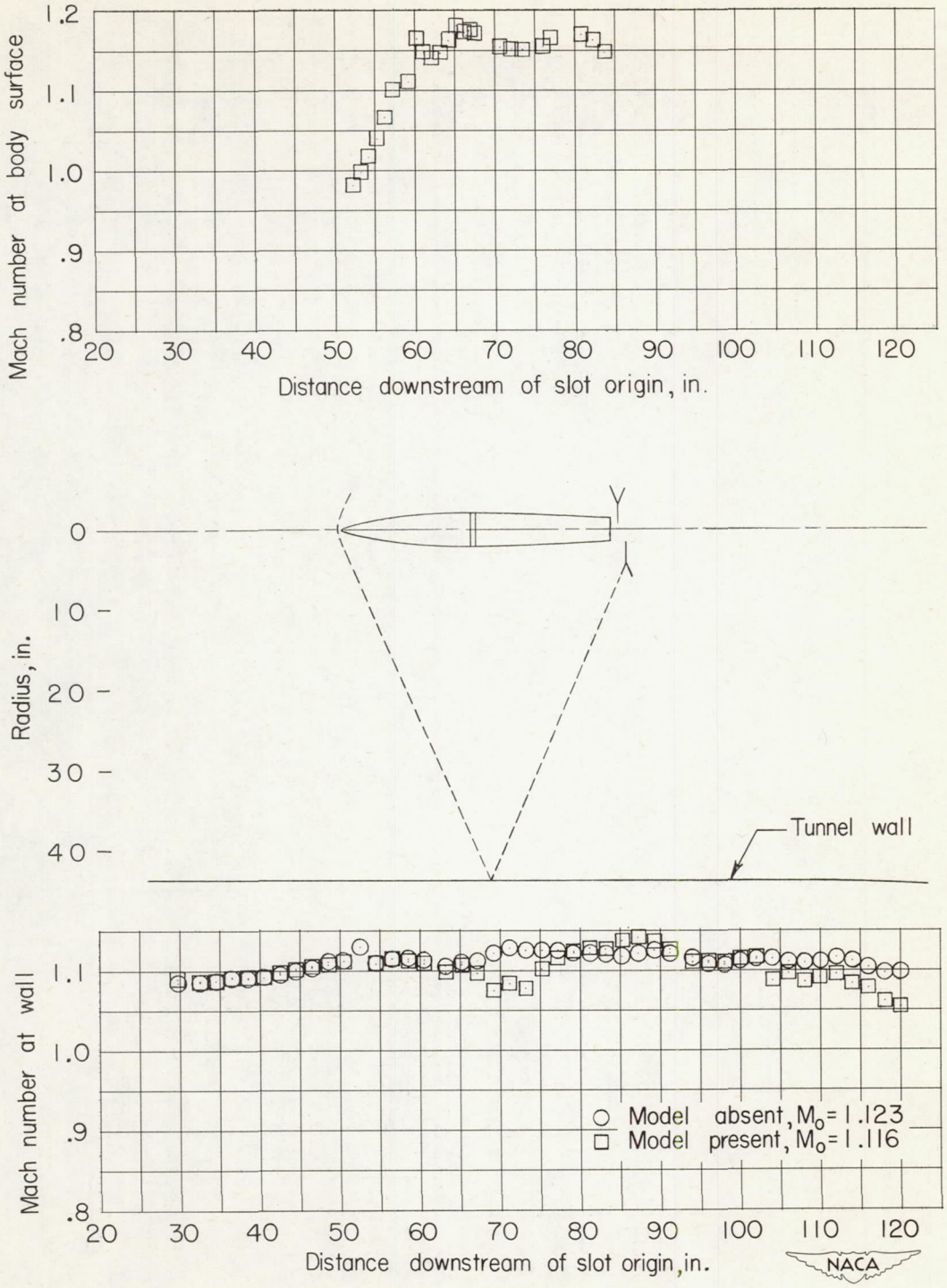

(i) $M_o \approx 1.12$.

Figure 8.- Concluded.

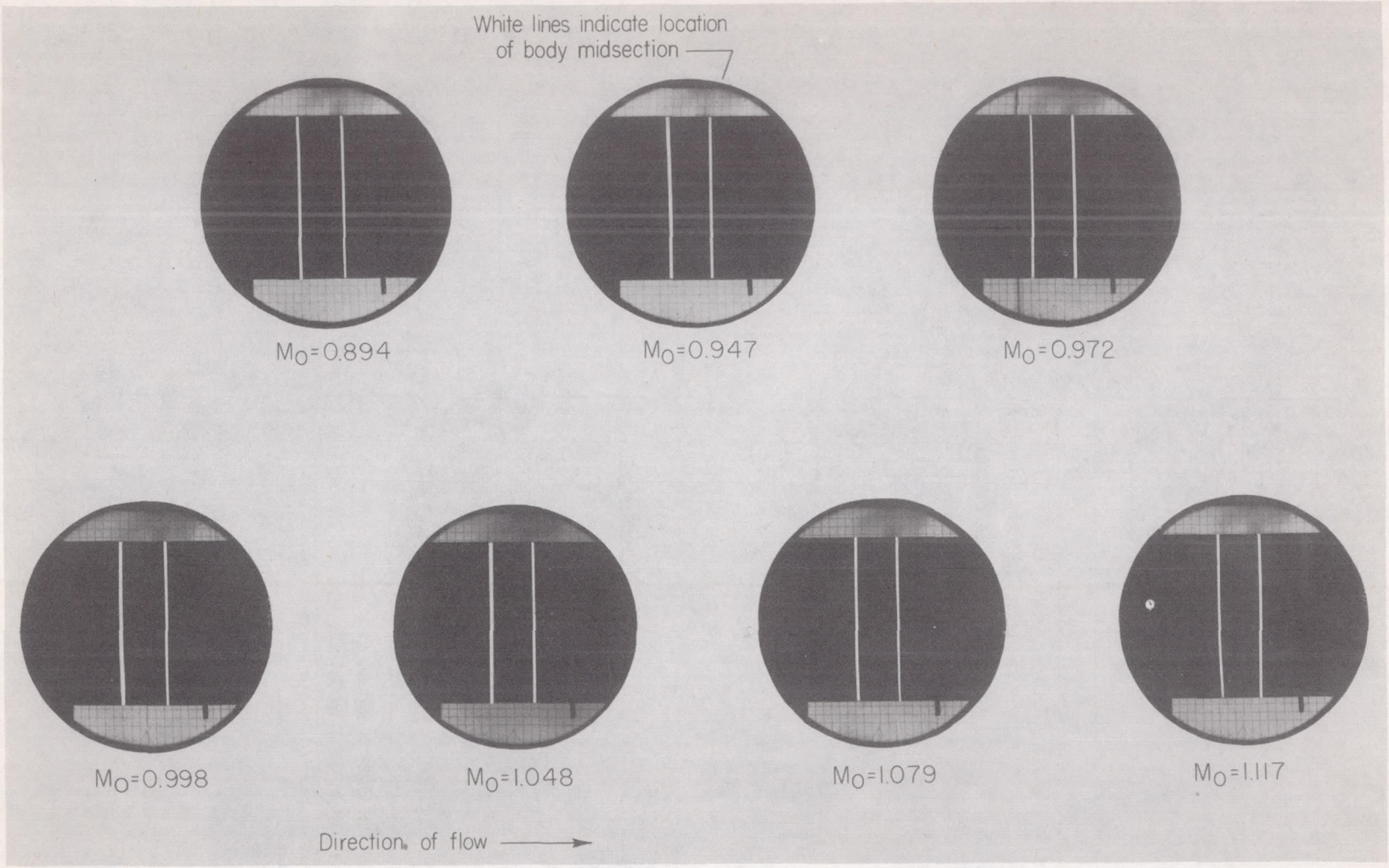

(a) D = 8 inches.

Figure 9.- Schlieren photographs. L-76151

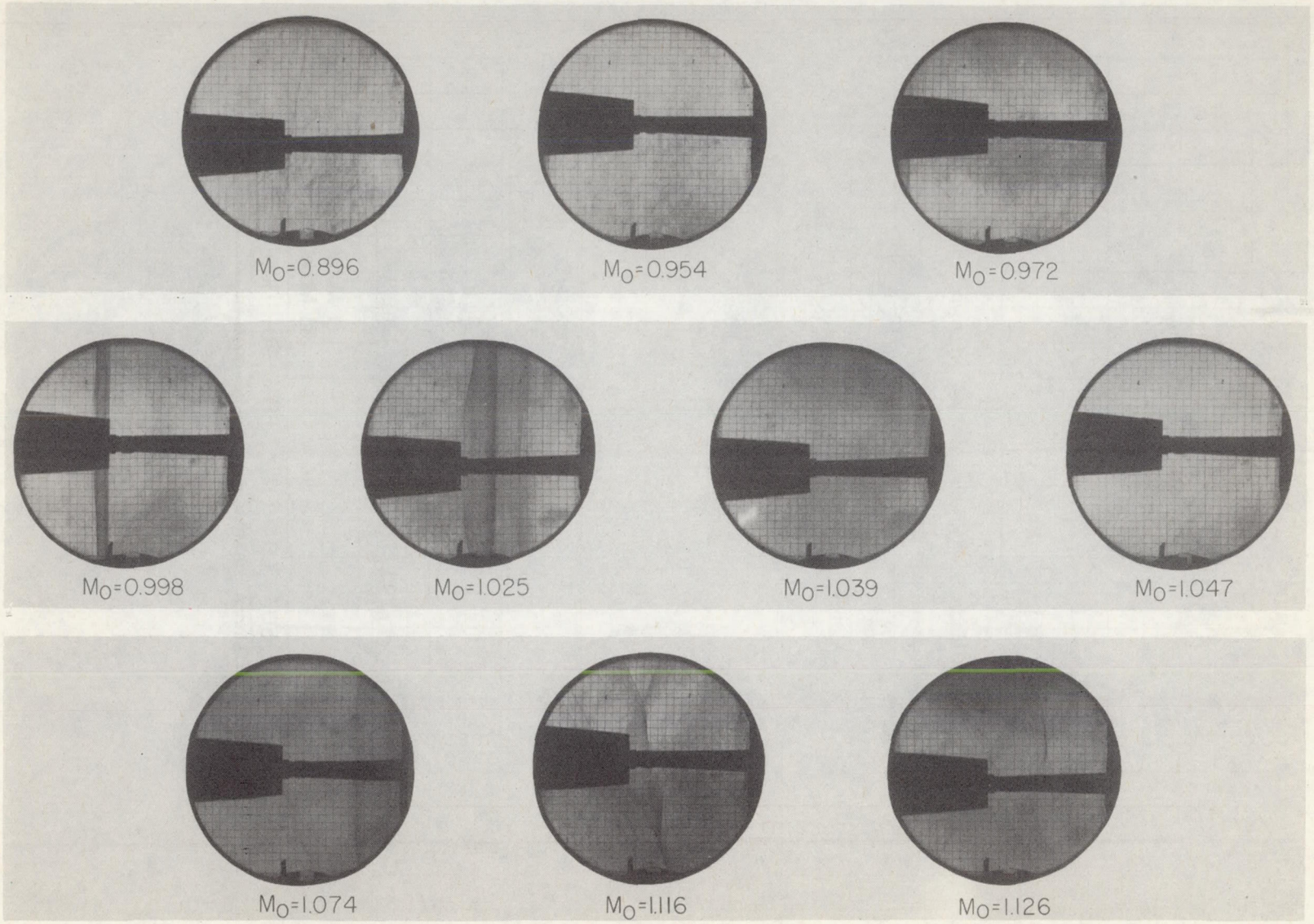

(b) D = 4 inches.

Figure 9.- Concluded.

NACA L-76152

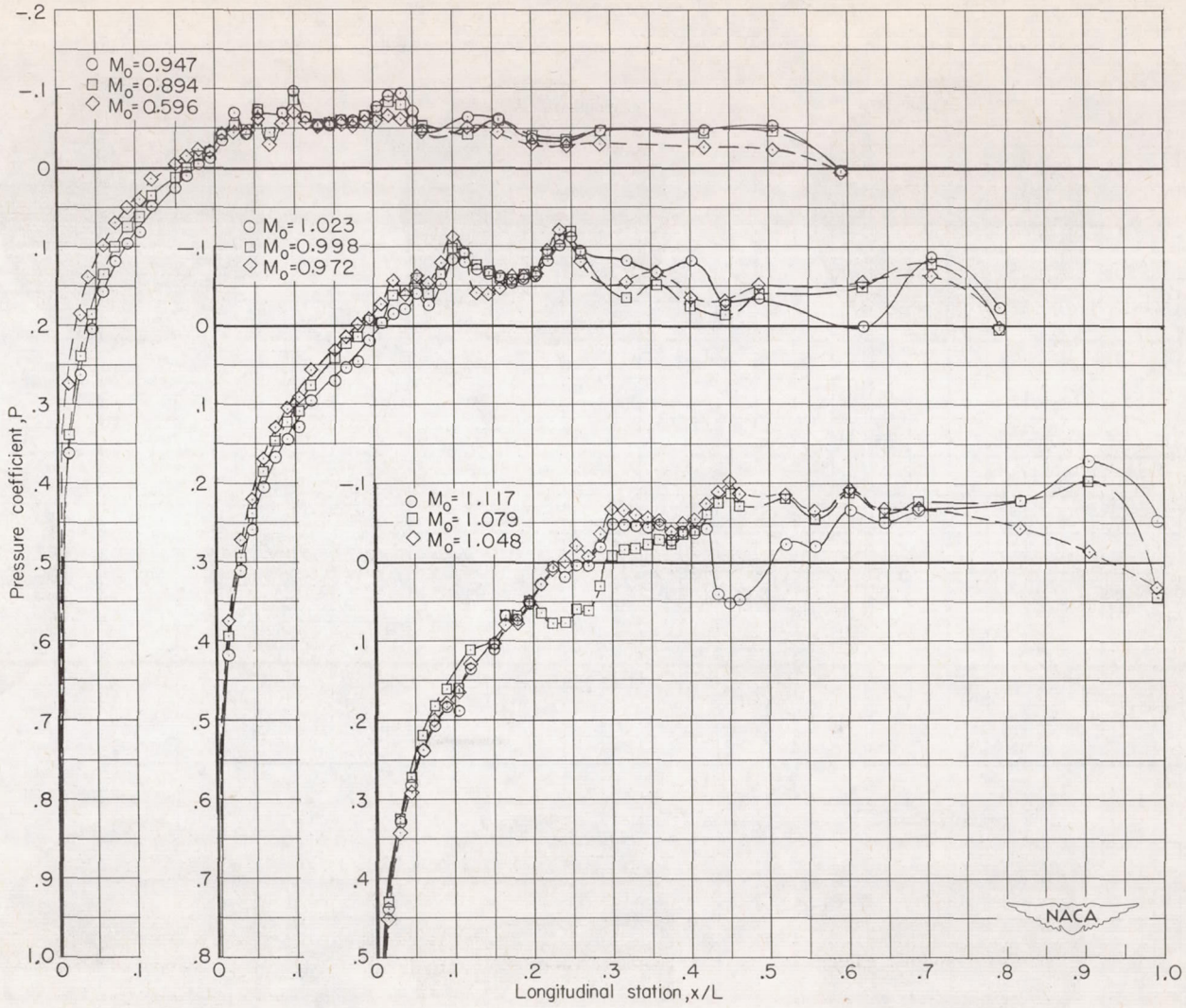

Figure 10.- Mach number effect on surface pressure distributions. D = 8 inches.

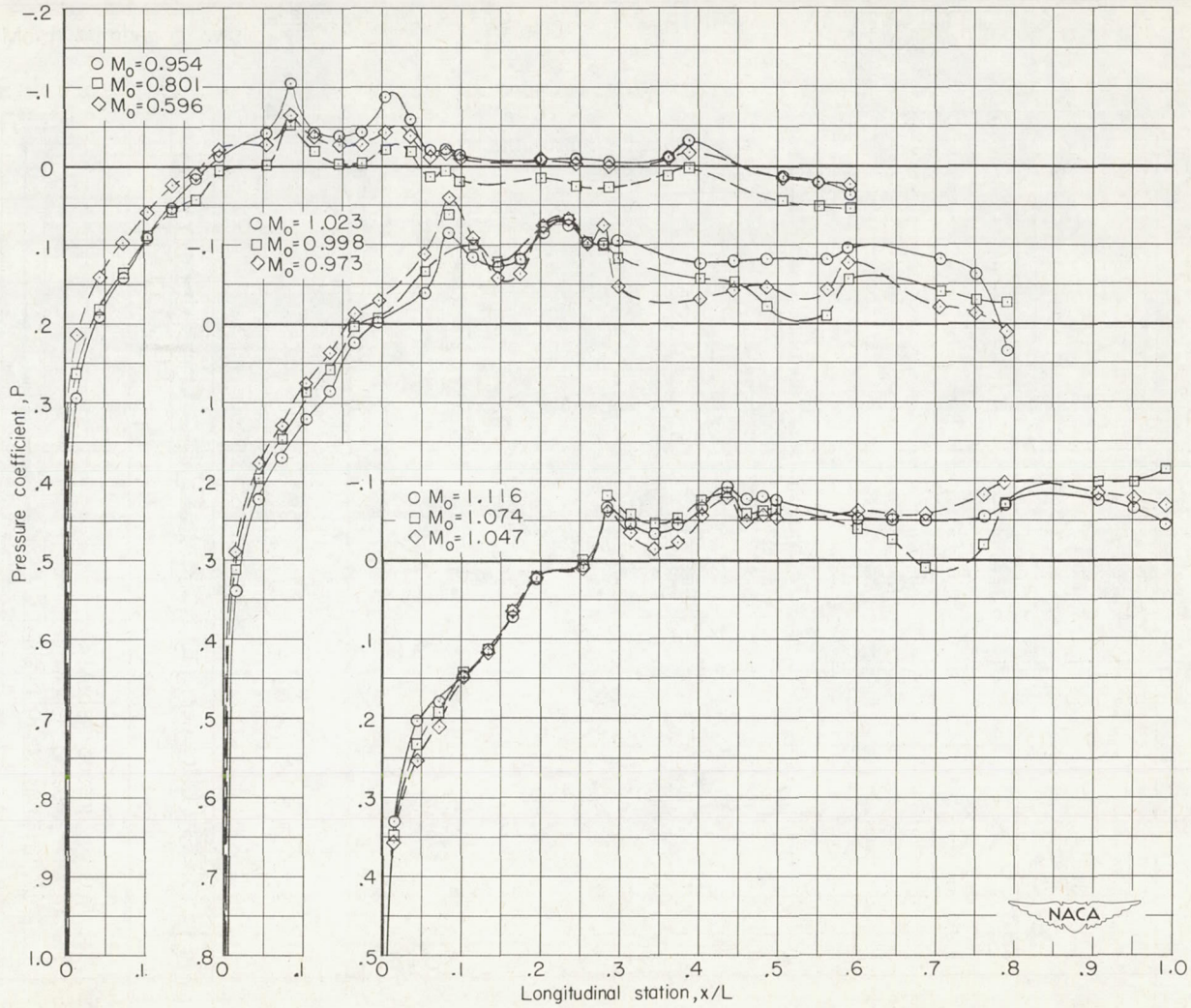

Figure 11.- Mach number effect on surface pressure distributions.
D = 4 inches.

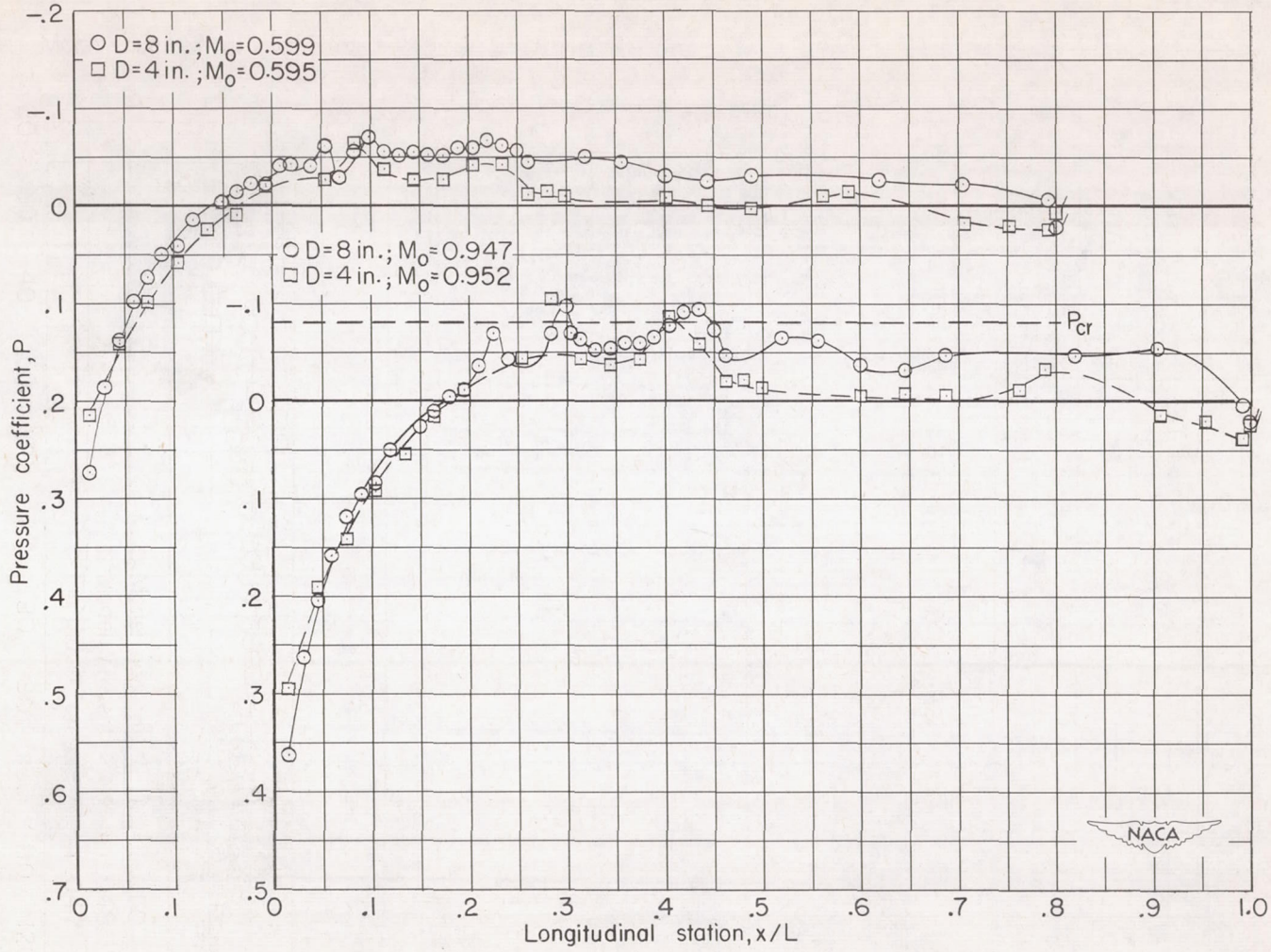

(a) M ≈ 0.597 and 0.950.

Figure 12.- Effect of model size on pressure distribution.

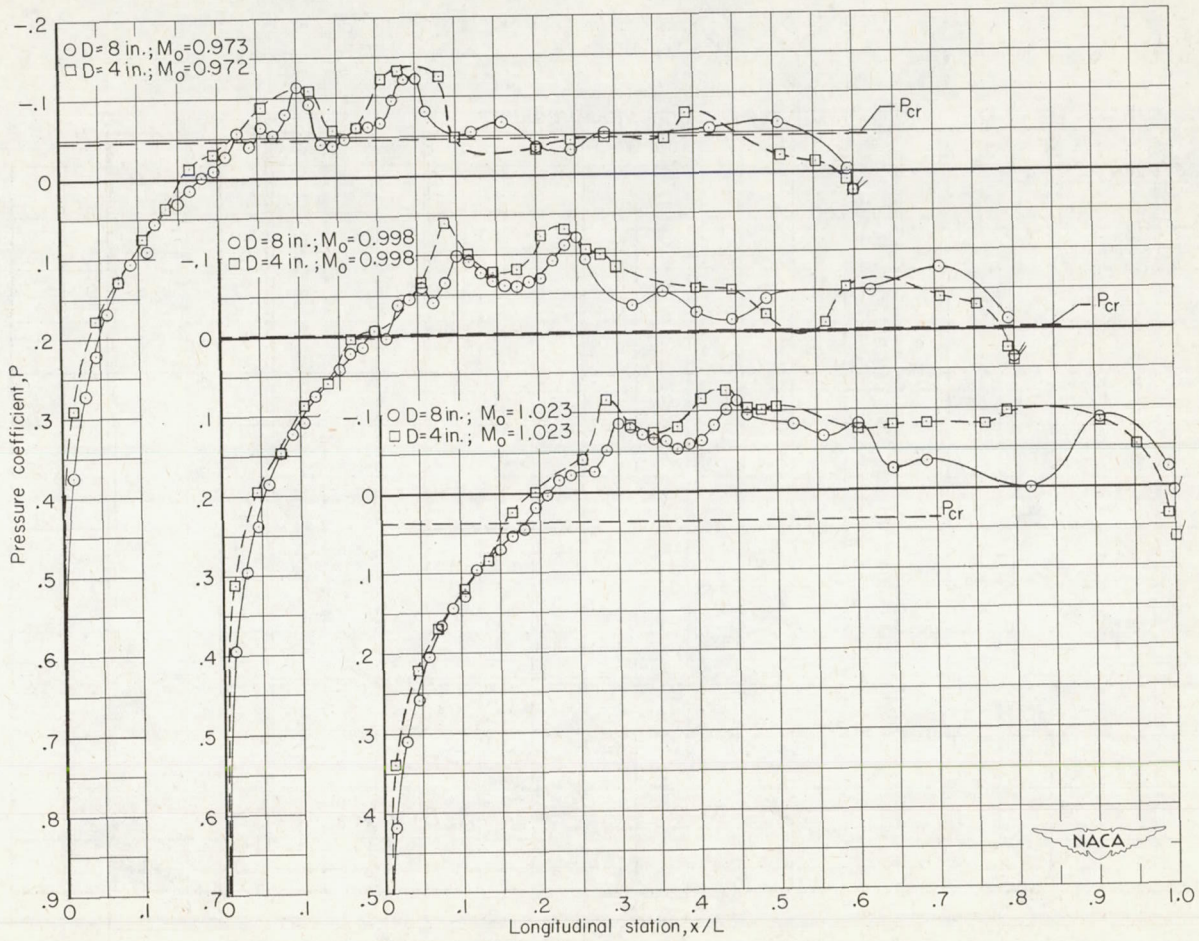

(b) M ≈ 0.973, 0.998, and 1.023.

Figure 12.- Continued.

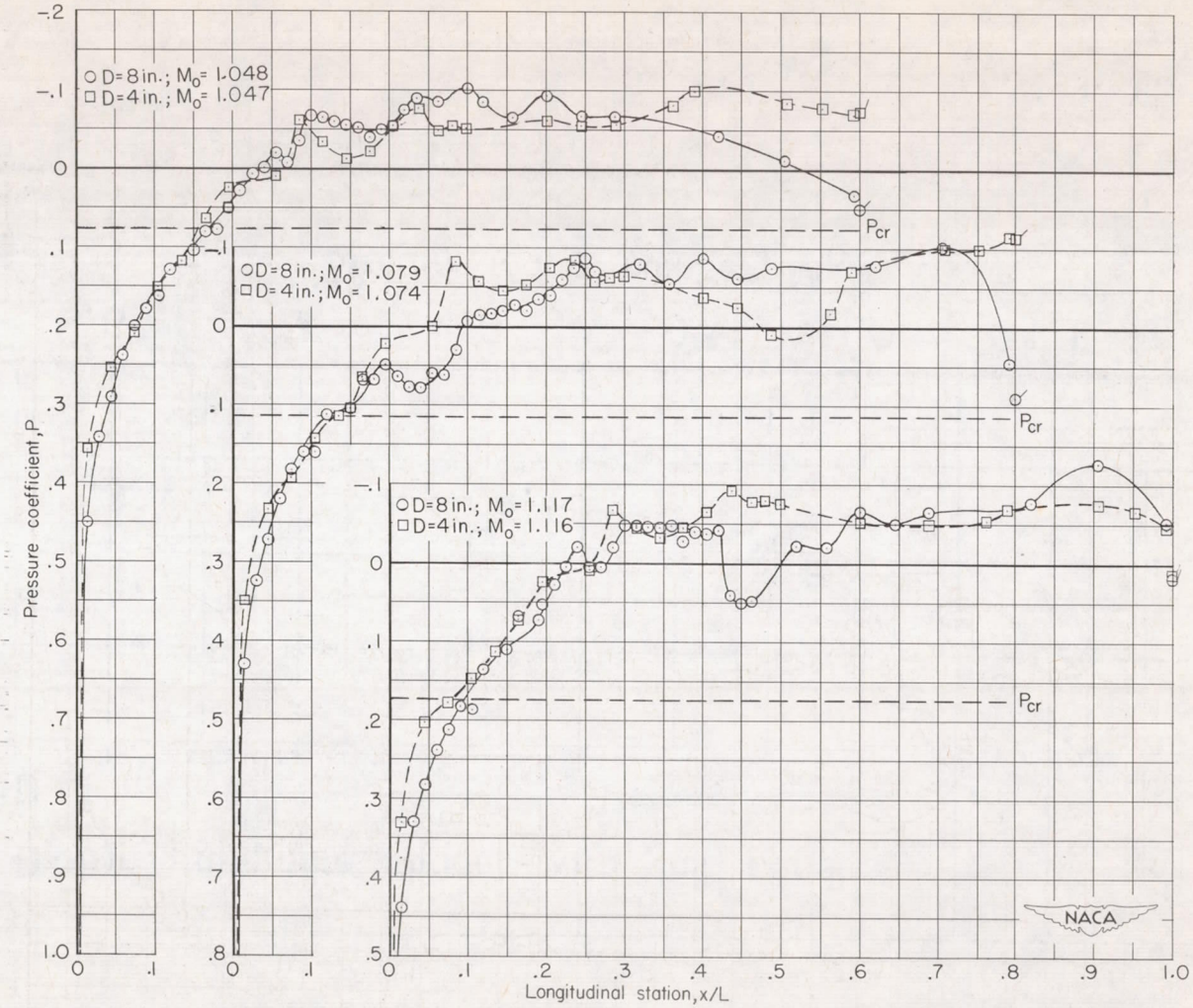

(c) M ≈ 1.048, 1.077, and 1.117.

Figure 12.- Concluded.

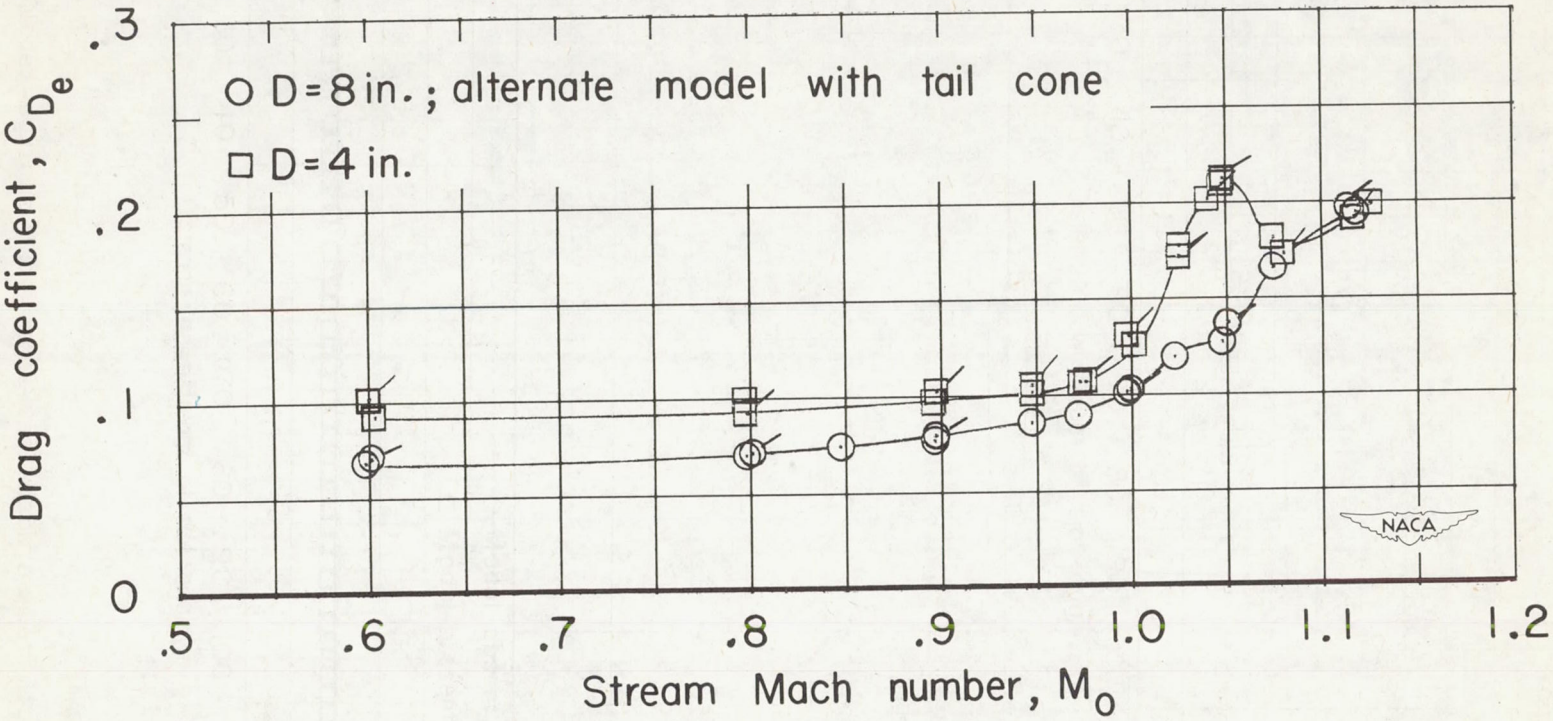

Figure 13.- Effect of transition strip on external drag. (Flagged symbols indicate transition fixed.)

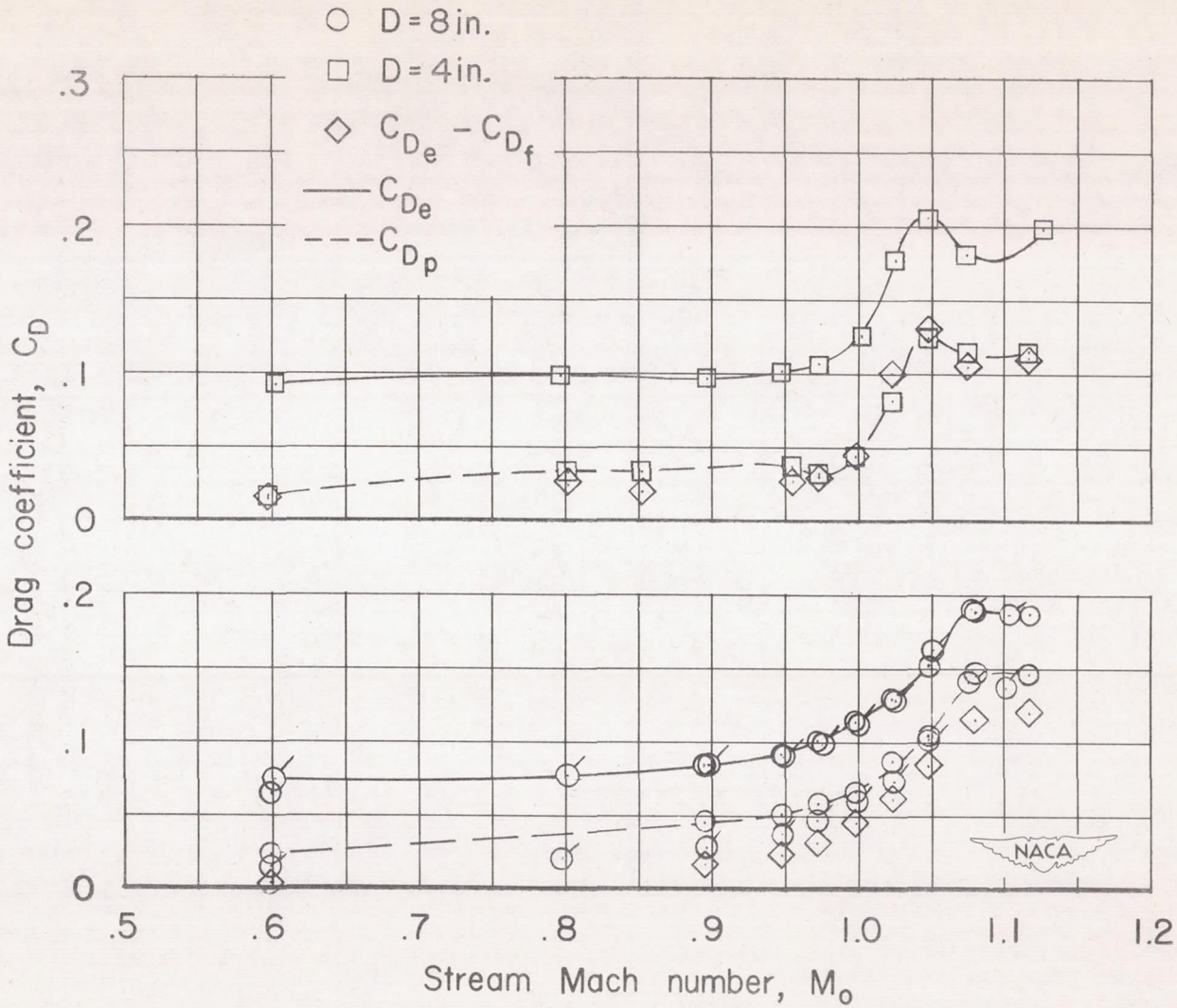

Figure 14.- Comparison of drag obtained from balance and pressure distributions. (Flagged symbols indicate alternate model.)

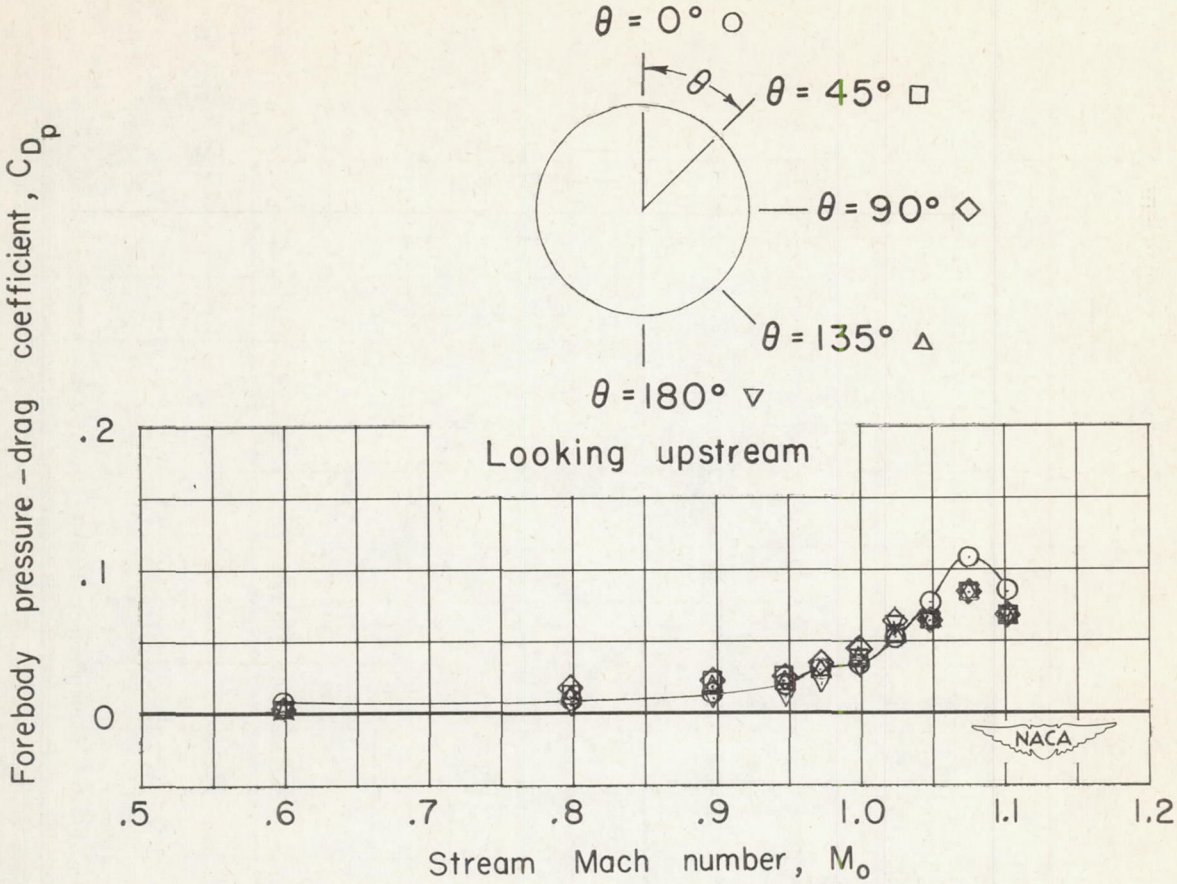

Figure 15.- Peripheral variation of integrated pressure drag from alternate model.

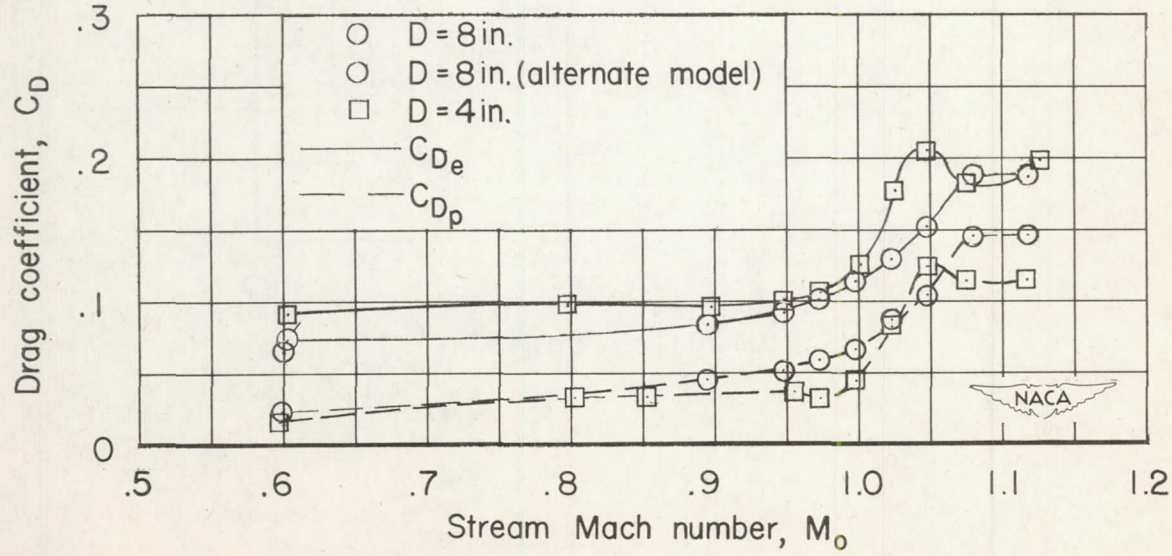

Figure 16.- Effect of body size on total and pressure drag.

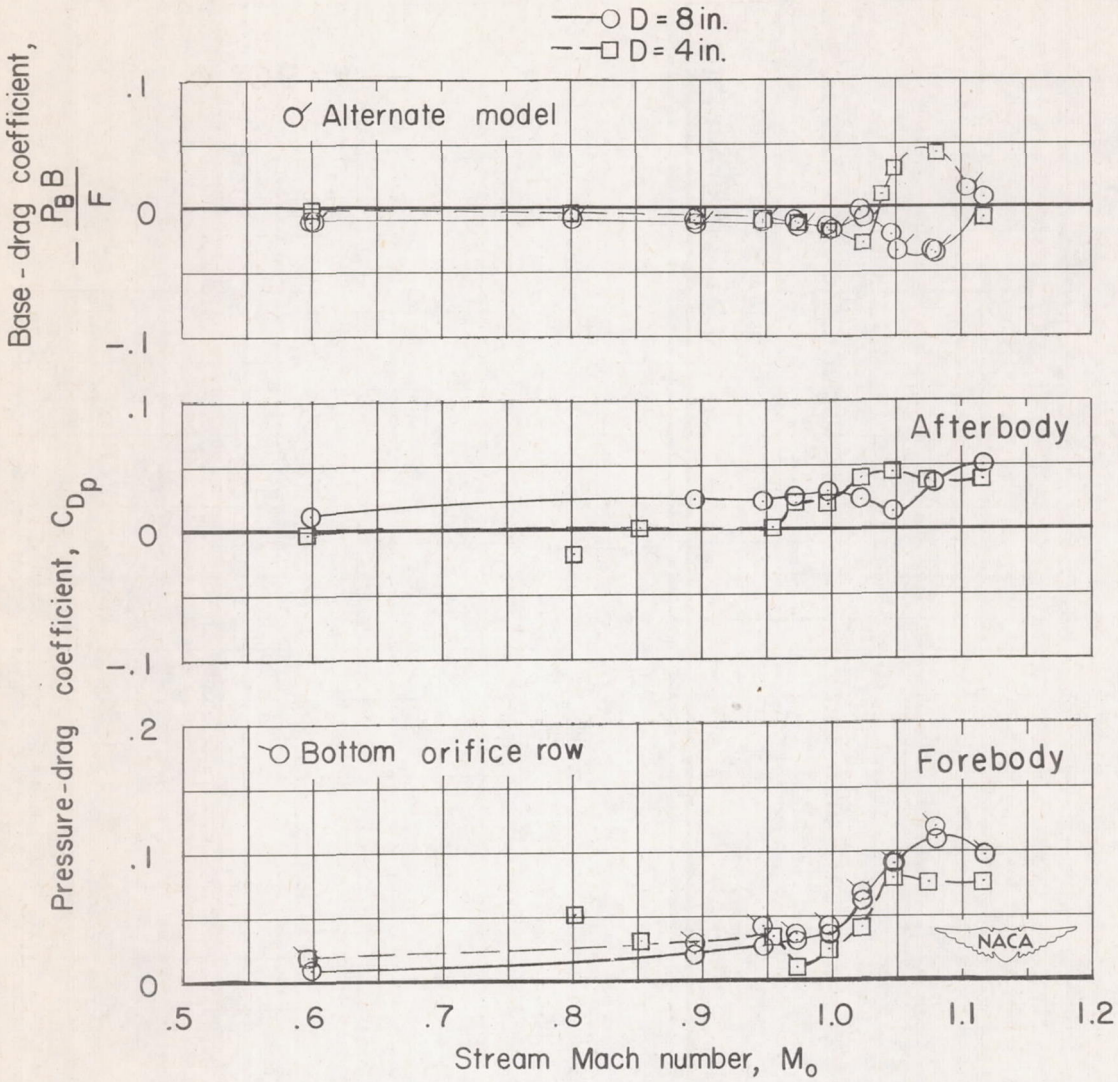

Figure 17.- Drag components.

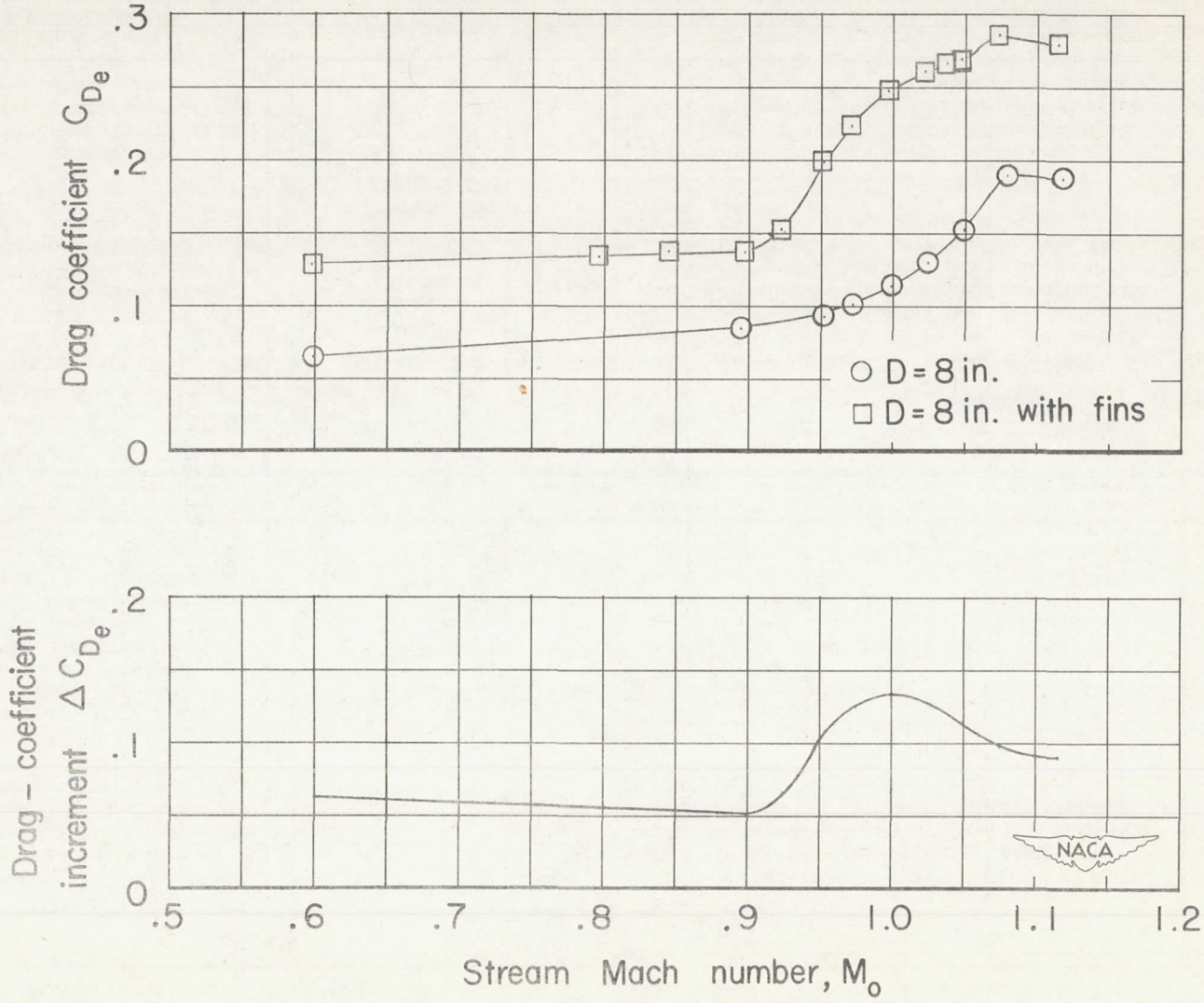

Figure 18.- Effect of tail fins on body drag.